Comparing various numerical coupling methods using a 1D Stefan problem

DISSERTATION WITH THE AIM OF ACHIEVING A DOCTORAL DEGREE AT THE
FACULTY OF MATHEMATICS, INFORMATICS AND NATURAL SCIENCES
DEPARTMENT OF EARTH SCIENCES AT UNIVERSITÄT HAMBURG
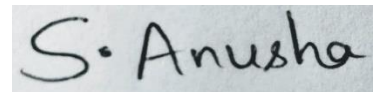
SUBMITTED BY ANUSHA SUNKISALA

2022 IN HAMBURG

Department of Earth Sciences	
Date of Oral Defense	18.10.2022
Reviewers	Prof. Dr. Jörn Behrens Dr. Konrad Simon
Members of the examination commission	Prof. Dr. Jörn Behrens Prof. Dr. Dirk Gajewski Prof. Dr. Felix Ament Dr. Konrad Simon Dr. Frank Lunkeit
Chair of the Subject Doctoral Committee Earth System Sciences	Prof. Dr. Hermann Held
Dean of Faculty MIN	Prof. Dr. Heinrich Graener

Eidesstattliche Versicherung

Hiermit erkläre ich an Eides statt, dass ich die vorliegende Dissertationsschrift selbst verfasst und keine anderen als die angegebenen Quellen und Hilfsmittel benutzt habe.

Ort, den   Unterschrift
Karlsruhe, 04.04.2022

Abstract

In general, coupling in a climate model is performed by exchanging fluxes between its model components through a software called "coupler". However, it is unclear whether this coupling strategy provides a consistent solution. Therefore, our study is motivated by a Schwarz iterative method, which provides a stable and consistent coupling solution. In order to implement this method, we considered a simple 1D test case called Stefan problem, where a domain is divided into two subdomains (say liquid and solid domains) with a moving interface called Stefan condition between them. The solution of Stefan problem is considered as a reference to our coupling methods. We implemented two coupling methods (loose and tight) and derived a coupling equation which is different from the Stefan problem. The liquid and solid domains are determined by diffusion equation with different diffusion coefficients. As we are dealing with a moving interface for our coupling methods, a coupling equation is derived based on first principle approach. We considered a grid point overlap between the subdomains and called it as loose coupling, which is similar to non-overlapping Schwarz method. In addition, we implemented tight coupling, similar to overlapping Schwarz method, where we considered five grid point overlap between the sub-domains in order to increase the overlap region. In loose and tight coupling, the diffusion equations for liquid and solid domains are discretized using forward in time and centered difference in space. However, the fluxes in the loose and tight coupling methods are discretized using low order and higher order finite difference method respectively. We then implemented iterative method to update the boundary conditions at the interface and interpolation to compute the new interface position. The results of loose and tight coupling methods are compared to the solution of Stefan problem. Also, in our study, we discussed how the different values of parameters in the coupling equation effects the solution of loose and tight coupling methods.

Zusammenfassung

Im Allgemeinen erfolgt die Kopplung in einem Klimamodell durch den Austausch von Flüssen zwischen den Modellkomponenten über eine Software, einen Koppler. Es ist jedoch unklar, ob diese Kopplungsstrategie eine konsistente Lösung bietet. Daher ist unsere Studie durch eine iterative Methode von Schwarz motiviert, die eine stabile und konsistente Kopplungslösung liefert. Um diese Methode zu implementieren, haben wir einen einfachen 1D Testfall, das so genannte Stefan-Problem, betrachtet, bei dem ein Rechengebiet in zwei Untergebiete (z. B. ein liquides und ein solides Gebiet) mit einer beweglichen Grenze, definiert durch die so genannte Stefan Bedingung, unterteilt ist. Die Lösung des Stefan-Problems wird als Referenz für unsere Kopplungsmethoden betrachtet. Wir haben zwei Kopplungsmethoden (eine schwache und steife) implementiert und eine Kopplungsgleichung abgeleitet, die sich vom Stefan-Problem unterscheidet. Die jeweiligen liquiden und soliden Bereiche werden durch eine Diffusionsgleichung mit unterschiedlichen Diffusionskoeffizienten bestimmt. Da wir es bei unseren Kopplungsmethoden mit einer beweglichen Grenzfläche zu tun haben, wird eine Kopplungsgleichung auf der Grundlage eines grundlegenden physikalischen Prinzips hergeleitet. Wir haben eine Gitterpunktüberlappung zwischen den Teilgebieten berücksichtigt und sie als schwache Kopplung (loose coupling) bezeichnet, die der nicht überlappenden Schwarz-Methode ähnelt. Darüber hinaus haben wir eine steife Kopplung (tight coupling) implementiert, die der überlappenden Schwarz-Methode ähnelt, bei der wir eine Überlappung von fünf Gitterpunkten zwischen den Unterdomänen berücksichtigen, um den Überlappungsbereich zu vergrößern. Bei der schwachen und der steifen Kopplung werden die Diffusionsgleichungen für die jeweiligen fluiden und soliden Teilgebiete durch Vorwärtsdifferenzen in der Zeit und zentrierte finite Differenzen im Raum diskretisiert. Die in den Flüssen auftretenden Ableitungen in den Methoden der schwachen und steifen Kopplung werden jedoch mit Finite-Differenzen-Methoden niedriger Ordnung bzw. höherer Ordnung diskretisiert. Wir haben weiterhin eine iterative Methode zur Aktualisierung der Randbedingungen an der Schnittstelle und eine Interpolation zur Berechnung der neuen Schnittstellenposition eingeführt. Die Ergebnisse der Methoden mit schwacher und steifer Kopplung werden mit der Lösung des Stefan-Problems verglichen. Schließlich haben wir untersucht, wie sich die verschiedenen Parameterwerte in der Kopplungsgleichung auf die Lösung unter der schwachen und steifen Kopplungsmethode auswirken.

Contents

Figures

Figure

Nomenclature

u	temperature
k_l	diffusion coefficient for liquid phase
k_s	diffusion coefficient for solid phase
H_f	latent heat
ρ	density
$s(t)$	position of the interface
Δt	time step
Δx	spatial step
f_l	liquid flux
f_s	solid flux
u_l	initial temperature for liquid
u_s	initial temperature for solid
u_m	melting temperature
i_b	index of the interface
St_l	Stefan number for liquid, $St_l = \frac{u_l - u_m}{L}$
St_s	Stefan number for solid, $St_s = \frac{u_m - u_s}{L}$
v	parameter, $v = \sqrt{\frac{k_l}{k_s}}$
ξ	similarity variable
$erf(\xi)$	error function
$erfc(\xi)$	complementary error function,

ip	grid point at left hand side of interface
$ip+1$	grid point at right hand side of interface
u_{ip}	temperature at grid point ip
u_{ip+1}	temperature at grid point ip+1
$\mathcal{L}_{atm}$	partial operators to the system of equations for atmosphere model
$\mathcal{L}_{oce}$	partial operators to the system of equations for ocean model
Ω	whole domain
Ω_{atm}	atmosphere as sub-domain
Ω_{oce}	ocean as sub-domain
Γ	interface
f_{atm}, f_{oce}	forcing terms

Chapter 1

Introduction

1.1   Motivation

In recent years, various climate models and couplers have been developed. A typical Earth System Model (ESM) is coupled with various model components, such as atmosphere, ocean, land, sea ice etc [1], [2], [3], [4], [5], [6]. Some of the examples of an ESM are: A Community Climate System Model (CCSM) developed at the National Center for Atmospheric Research (NCAR). A Community Earth System Model (CESM), which is an extension of CCSM provides various options like additional land - ice component, land - ocean biogeochemistry etc. These climate models use various couplers like OASIS(Ocean Atmosphere Sea Ice Soil) [7], [8] and its various versions (OASIS3, OASIS3-MCT, OASIS3-MCT3.0, OASIS3-MCT4.0), YAC(Yet Another Coupler), FMS(Flexible modeling system) etc. Although the implementation of these couplers are different, they provide similar functions like managing data transfer between model components, interpolating the coupling data between different grids and coordinating the model components. However, these couplers have some constraints related to conservation, synchronisation and consistency as explained in [9]. Moreover, these coupling methods do not provide a converging solution to the coupling problem since they are equivalent in performing single iteration [9], [10], [11]. The solution for such problems is addressed by Schwarz iterative method, which can yield a stable and consistent coupling method [10]. Therefore, our study is motivated by Schwarz iterative method and the hypothesis of this study is to understand complex coupling process

and we attempt to see if the iterative method could improve the coupling solution. Since the climate models are quite complex to understand, we consider 1D equations to perform this method. The research with Schwarz iteration with a fixed interface is already been done for 1D equations [10], [11], [12], [13], [14] and later extended to complex atmosphere and ocean coupling [9]. These studies are conducted only with a fixed interface between the subdomains. We also implemented Schwarz method to 1D poisson and diffusion equation with a fixed interface, explained in Appendix A as a preliminary result. But, in a real world, the interface between two models is not fixed. Some of the examples are: The sea ice forms the interface between the ocean and the atmosphere for extended periods of time [15], [16]. The movement of sea ice, which results in its melting or formation, depends on the exchange of solar radiation, salinity, heat and other factors between atmosphere and ocean. The ice movement reflects the export and loss of ice into the ocean through surface meltwater fluxes [17]. Also, the movement caused by drifting of snow, depends on factors like near-surface wind speeds, surface snow density, associated threshold friction velocity, meltwater runoff etc [18]. The glacier movement caused due to the interaction between the gravitational driving force of downward ice movement and the resistance encountered at the bed and margins [19]. As there are difficulties in assessing the interface of ice-bed in a glacier, surface movement of a glacier is used as a proxy to represent the glacier motion [20]. The glacier velocity is explained in [21] to understand the surface morphology of both clean-ice and debris-covered glacier. Hence, it is important to investigate coupling strategies to a moving interface. According to our knowledge, research has not yet done on Schwarz iterations with a moving interface. As a result, in our study we considered Schwarz iterative method to couple 1D diffusion equation for two subdomains with different diffusion coefficients and a moving interface between them.

Why diffusion equation?

From the literature review, we found a 1D test case called "Stefan problem" [24], [23], [25], [22], which is a prototype for some of the examples mentioned above (sea-ice interface, drifting

of snow and the movement of glacier). The solution of the Stefan problem is simple yet conserved and therefore we consider it as reference to our coupling methods. Stefan problem involves the distribution of heat in a phase changing medium, which uses a diffusion equation and a Stefan condition to understand the heat flow and change of phase respectively. On the basis of Stefan problem, we use diffusion equation for the subdomains in order to implement our coupling methods.

1.2   Present Coupling methods

In this chapter, we discuss the present coupling methods, like using a coupler (for example OASIS coupler) [26], which couples different model components, described in 1.2.1. Also in section 1.2.2, we discuss the 1D coupling, which couples 1D diffusion equation for atmosphere and land with fixed interface using a exchange grid [27] and by using Schwarz iterations [10] with a fixed interface. In section 1.2.3, we discuss the synchronous and asynchronous coupling methods with different time scales [9]. In section 1.2.4, we describe the Schwarz iterative method based on [9], which solves the problems obtained by synchronous and asynchronous coupling.

1.2.1   Coupling using a Coupler

As mentioned in section 1.1, there are various couplers being used, however their main function is to exchange fluxes between various model components and to interpolate the coupling fields. Here we discuss the OASIS coupler used in Sein et.al., [26], where it couples various components like atmosphere, marine bio-geochemistry, river runoff along with ocean and ice components. The figure 1.1 shows the coupling between REMO [28], [1], a atmospheric component and a ocean component, MPIOM [2], [5], [29]. Here, the ocean model needs to run in both coupled subdomain and as a stand-alone model simultaneously. In the coupled sub-domain, the ocean model receives the heat, freshwater, and momentum fluxes from the atmosphere model at specified time step, whereas in uncoupled sub-domain, the

surface boundary condition fields are calculated from the predefined atmospheric fields using Bulk formula. Now, the atmosphere model receives fluxes from the ocean model (both coupled and uncoupled mode) which provides sea surface conditions [30], [31]. To summarise this coupling process, a coupler interpolates the coupling fields in order to compute the fluxes at the interface and provides input to each sub-component of the model. However, still it is unclear if this coupling strategy provides a consistent framework for coupling components of climate models.

The aim of our study is not to prove that this coupling process is incorrect, but we attempt to see if we could improve the coupling solution by Schwarz iteration method. However, coupling in an earth system model is quite complex to understand and therefore, we considered a simple test case where we implement Schwarz iterative method to couple two 1D diffusion equations with different diffusion coefficients and a moving boundary at the interface further described in chapter 3 and 4.

1.2.2   1D Coupling with a fixed interface

Here, we describe 1D coupling with a fixed interface using a exchange grid based on Balaji et al., 2008 [27]. It considers vertical diffusion of temperature in a coupled atmosphere-land system. Vertical diffusion in atmosphere model is discretized using implicit method and fluxes are also computed implicitly at the interface to improve the stability.

$$\frac{\partial u}{\partial t} = k \frac{\partial^2 u}{\partial z^2} \tag{1.1}$$

$$\frac{(u_i^{n+1} - u_i^n)}{\Delta t} = \frac{k}{(\Delta x)^2}(u_{i+1}^{n+1} - 2u_i^{n+1} + u_{i-1}^{n+1}) \tag{1.2}$$

$$Au^{n+1} = u^n \tag{1.3}$$

This is a tridiagonal matrix inversion which was solved using an up-down sweep. Some of the layers are considered in atmosphere and others are in land. This paper [27] uses a exchange grid as an independent model component to compute the fluxes at the surface boundary
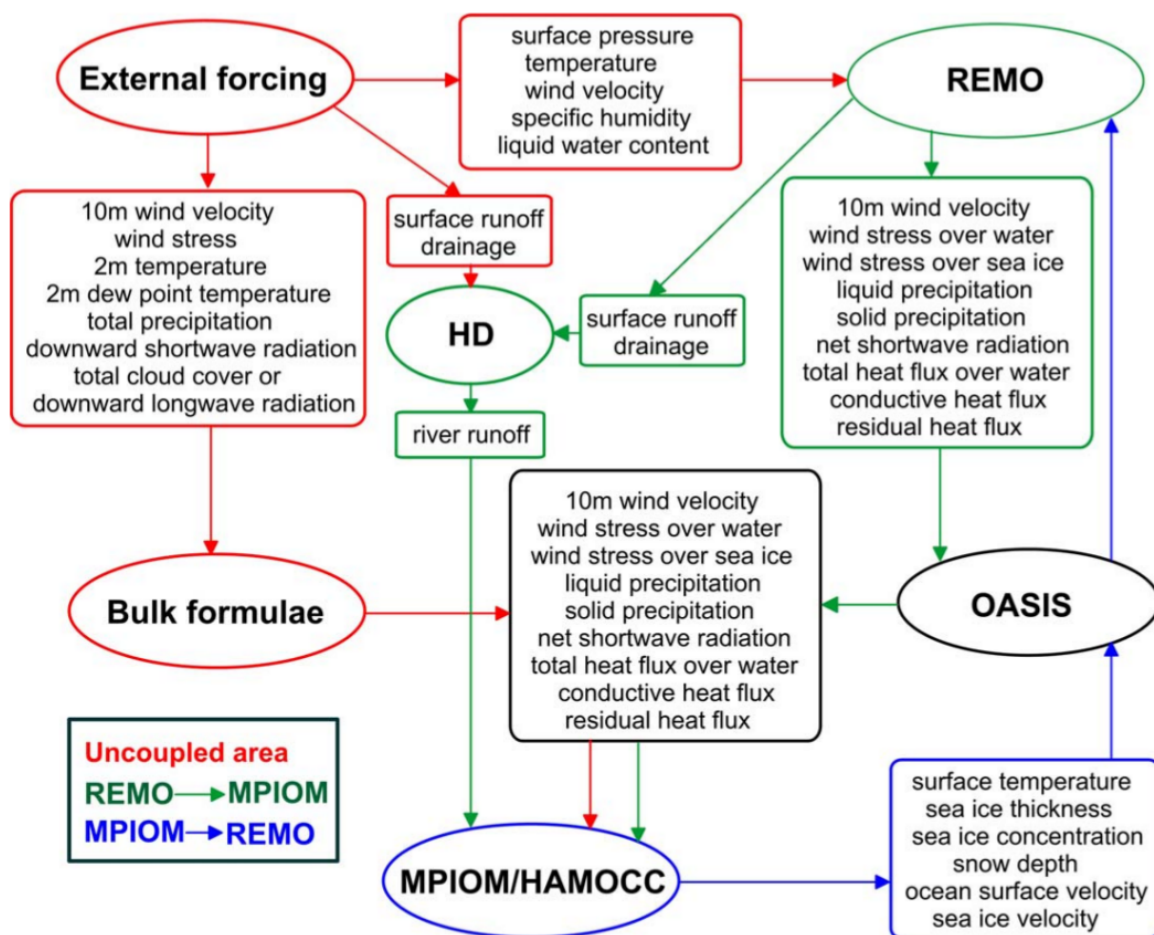
Figure 1.1: Coupling scheme from [26]. Red colour denotes the prescribed forcing used as lateral boundary conditions for REMO and as surface forcing for MPIOM in the uncoupled area. The workflow of heat, momentum, and mass fluxes from the atmosphere (REMO) to the ocean (MPIOM) in the coupled area is marked with green. The data flow from MPIOM to REMO is marked with blue.

layer. The diffusion equation is partially solved in the atmosphere model and quantities are sent to the exchange grid to compute fluxes. Now the ocean model receives the fluxes from the exchange grid and calculates diffusion for the ocean(other sub-domain) and return values to the exchange grid. However, we understood from the literature [10], [11], [9] that use of Schwarz iteration converges to the exact solution, therefore we now follow some of the research conducted using Schwarz method to couple 1D diffusion equation with a fixed interface between the sub-domains [10]. This study [10] uses various interface conditions like Dirichlet-Neumann, Neumann-Robin and Robin-Robin with various ratios of diffusion coefficients. The results shows that the coupling solution not only depends on interface condition but also on the ratio of diffusion coefficients [10]. Moreover, when the ratio between the diffusion coefficients is increased, the coupling solution becomes less sensitive to the use of interface condition. Therefore, in our study, we also performed numerical tests for coupling methods (named as loose and tight, further explained in chapter 3) with various ratios of diffusion coefficients. Also, coupling of 1D diffusion equation using a moving interface, which is a more "realistic" case is attempted in our study. However, we needed to derive a coupling equation (3.15), in section 3.4 as we are dealing with a moving interface.

1.2.3 Coupling of different time scales

In this section, we describe the usual coupling methods used in global and regional climate models. According to Lemarié et al., 2015, the existing coupling methods like asynchronous and synchronous methods do not provide a exact coupling solution, but an approximation [9]. Therefore, it is important to understand these coupling methods (1.2.3.1 and 1.2.3.2) and their issues which are solved by using Schwarz iterative method (1.2.4).

Consider $\mathcal{L}_{\mathrm{atm}}$ and $\mathcal{L}_{\mathrm{oce}}$ as the partial operators to the system of equations for atmosphere and ocean models respectively. Let the atmosphere domain be Ω_{atm} and Ω_{oce} be the ocean domain with a common interface Γ. Let Ω be the union of atmopshere and ocean domains, $\Omega = \Omega_{\mathrm{atm}} \cup \Omega_{\mathrm{oce}}$, with external boundaries as $\partial\Omega_{\mathrm{atm}}^{\mathrm{ext}}$ and $\partial\Omega_{\mathrm{oce}}^{\mathrm{ext}}$. The below equations are

considered from the literature [9].

$$\mathcal{L}_{\text{atm}}U^a = f_{\text{atm}} \quad \text{in} \quad \Omega_{\text{atm}} \times [0, \mathcal{T}], \tag{1.4}$$

$$\mathcal{B}_{\text{atm}}U^a = g_{\text{atm}} \quad \text{in} \quad \partial\Omega_{\text{atm}}^{\text{ext}} \times [0, \mathcal{T}], \tag{1.5}$$

$$\mathcal{F}_{\text{atm}}U^a = F_{\text{oa}}(U^o, U^a, \mathcal{R}) \quad \text{on} \quad \Gamma \times [0, \mathcal{T}], \tag{1.6}$$

$$\mathcal{L}_{\text{oce}}U^o = f_{\text{oce}} \quad \text{in} \quad \Omega_{\text{oce}} \times [0, \mathcal{T}], \tag{1.7}$$

$$\mathcal{B}_{\text{oce}}U^o = g_{\text{oce}} \quad \text{in} \quad \partial\Omega_{\text{oce}}^{\text{ext}} \times [0, \mathcal{T}], \tag{1.8}$$

$$\mathcal{F}_{\text{oce}}U^o = F_{\text{oa}}(U^o, U^a, \mathcal{R}) \quad \text{on} \quad \Gamma \times [0, \mathcal{T}], \tag{1.9}$$

where $\mathcal{B}_{\text{oce}}$ and $\mathcal{B}_{\text{atm}}$ are the boundary operators, which provides initial and boundary conditions. In equations from (1.4) to (1.9), $U^a = (u_h^a, T^a)^t$ and $U^o = (u_h^o, T^o)^t$ are the state variables with u_h the horizontal velocity and T the (potential) temperature, whereas f_{atm} in (1.4) and f_{oce} in (1.7) are considered as forcing terms. F_{oa} is a function that allows the computation of air-sea fluxes. $\mathcal{F}_{\text{atm}}$ and $\mathcal{F}_{\text{oce}}$ are the interface operators, further explained in [9]. In further subsections, we discuss the coupling methods to solve (1.4) - (1.9). In sub-section 1.2.3.1, we discuss the first approach, called asynchronous coupling, which is based on the exchange of averaged fluxes between the models, whereas in sub-section 1.2.3.2, synchronous coupling is discussed where instantaneous fluxes are exchanged.

1.2.3.1 Asynchronous coupling

In most of the climate models, asynchronous coupling is used. In this method, total simulation time [0,T] is split into M smallest time windows $[t_i, t_{i+1}]$, i.e $[0,T] = \cup_{i=1}^M [t_i, t_{i+1}]$. Consider $\langle . \rangle_i$ as a temporal average over time window $[t_i, t_{i+1}]$. The algorithm below for atmosphere, ocean and coupling are taken from the literature [9].

$$\mathcal{L}_{\text{atm}}U^a = f_{\text{atm}} \quad \text{in} \quad \Omega_{\text{atm}} \times [t_i, t_{i+1}] \tag{1.10}$$

$$\mathcal{F}_{\text{atm}}U^a = F_{\text{oa}}(\langle U^o \rangle_{i-1}, U^a, \mathcal{R}) \quad \text{on} \quad \Gamma \times [t_i, t_{i+1}] \tag{1.11}$$

$$\mathcal{L}_{oce} U^o = f_{oce} \quad \text{in} \quad \Omega_{oce} \times [t_i, t_{i+1}] \tag{1.12}$$

$$\mathcal{F}_{oce} U^o = \langle \mathcal{F}_{atm} U^a \rangle_i \quad \text{on} \quad \Gamma \times [t_i, t_{i+1}] \tag{1.13}$$

In equation (1.11), the averaged ocean fluxes of previous time step i-1 are given to atmosphere model to advance from i to i+1. Now, the averaged atmosphere flux are applied to the ocean model at the same time interval, see in equation (1.13). However, the algorithm does not solve the original problem (1.4) - (1.9) because of the synchronicity issue. This is described in literature [9] as follows: synchronicity problem occurs as the values of the ocean component are not provided to the atmospheric component at same time interval, but at the next time interval.

1.2.3.2 Synchronous coupling

In synchronous coupling, ocean and atmosphere components exchange instantaneous fluxes at same time interval. If we consider the ocean step as Δt_o, such that $\Delta t_o = N \Delta t_a$, where t_a is the atmospheric step. The algorithm for ocean, atmosphere and coupling are taken from Lemarié et al., 2015 [9].

$$\mathcal{L}_{atm} U^a = f_{atm} \quad \text{in} \quad \Omega_{atm} \times [t_i, t_i + N \Delta t_a] \tag{1.14}$$

$$\mathcal{F}_{atm} U^a = \mathcal{F}_{oa}(U^o(t_i), U^a(t), \mathcal{R}(t)) \quad \text{on} \quad \Gamma \times [t_i, t_i + N \Delta t_a] \tag{1.15}$$

$$\mathcal{L}_{oce} U^o = f_{oce} \quad \text{in} \quad \Omega_{oce} \times [t_i, t_i + \Delta t_o] \tag{1.16}$$

$$\mathcal{F}_{oce} U^o = \mathcal{F}_{oa}(U^o(t_i), U^a(t_i), \mathcal{R}(t_i)) \quad \text{on} \quad \Gamma \times [t_i, t_i + \Delta t_o] \tag{1.17}$$

Although the above algorithm (1.14 - 1.17) may appear as the solution to the problem (1.4) - (1.9), but the algorithm (1.14 - 1.17) is difficult to implement from computational and numerical point of view. Also, from the stability analysis mentioned in Lemarié et al., 2015 [9], the numerical implementation of synchronous coupling can be unstable.

Since asynchronous and synchronous coupling have issues with respect to consistency, conservation and synchronisation (refer to Lemarié et al., 2015 [9] for further analysis), in section 1.2.4, these problems are solved using Schwarz iterations [10], [11], [9].

1.2.4   Schwarz iterative method

The idea of Schwarz method is to separate the original problem on $\Omega = \Omega_{atm} \cup \Omega_{oce}$ into sub problems on Ω_{atm} and Ω_{oce}, which can be solved separately. This is, however, true for what we have mentioned in the previous section as well. However, in this method, we assume that the system of $\mathcal{L}_{atm}U^a = f_{atm}$ together with $\mathcal{L}_{oce}U^o = f_{oce}$ on $\Omega_{atm} \cup \Omega_{oce}$ forms one wholistic system. In other words, we assume that we have a problem $\mathcal{L}U = f$ on Ω that can be decomposed into $\mathcal{L}_{atm}|_{\Omega_{atm}} \bigoplus \mathcal{L}_{oce}|_{\Omega_{oce}}$ and their corresponding solutions. An iterative process is then applied to achieve convergence to the solution of the original problem [13]. Schwarz methods were introduced for stationary problems (say for example Poisson equation), but later extended to time dependent problems to provide a global in time Schwarz method, refer to Blayo et al., 2007 [32], where optimized Schwarz method is applied for convective-diffusion problems with discontinuous coefficients. Also, this method is applied to diffusion equation with constant coefficients [10] and later extended for variable coefficients case [11]. Later, these methods ([10], [11]) developed by Lemarié are applied for ocean-atmosphere coupling [9], described in this section 1.2.4 to solve the coupling problem(1.4) - (1.9). Moreover, Schwarz method solves the problem of synchronicity mentioned in synchronous and asynchronous coupling, refer to stability analysis in section.3 in [9]. The iterative algorithm below is taken from the paper [9] is written as follows :

$$\mathcal{L}_{atm}U_k^a = f_{atm} \quad \text{in} \quad \Omega_{atm} \times [t_i, t_{i+1}], \tag{1.18}$$

$$\mathcal{F}_{atm}U_k^a = F_{oa}(U_{k-1}^o, U_k^a, \mathcal{R}_k) \quad \text{on} \quad \Gamma \times [t_i, t_{i+1}], \tag{1.19}$$

$$\mathcal{L}_{oce}U_k^o = f_{oce}, \quad \text{in} \quad \Omega_{oce} \times [t_i, t_{i+1}], \tag{1.20}$$

$$\mathcal{F}_{oce}U_k^o = \mathcal{F}_{atm}U_k^a \quad \text{on} \quad \Gamma \times [t_i, t_{i+1}], \tag{1.21}$$

where the subscript k denotes the iteration number. The first guess $U_{k=0}^o$ on $\Gamma \times [t_i, t_{i+1}]$ is generally taken from the converged solution on the previous time window $[t_{i-1}, t_i]$. When the convergence is reached, this algorithm gives the exact solution to the problem (1.4) - (1.9).

However, the Schwarz iterative method described in this section is basically for a non-moving interface and for Dirichlet boundary conditions. In our study, we had the problem, that we needed to deal with the fluxes over the boundary because of the moving boundary at the interface. In order to solve this problem, we changed the scheme, described in section 1.3.

1.3   1D Coupling with a moving interface

Research has been conducted on 1D coupling using a fixed interface [27] and Schwarz iterative method [10], [11], [9], explained in section 1.2.1. In our study, we implemented a moving interface which is more "realistic" test case compared to a fixed interface. Some of the examples of a moving interface are sea-ice interface between atmosphere and ocean, drifting of snow and the movement of a glacier.

In this section, we describe 1D coupling with a moving interface and Schwarz iterative method. In these coupling methods, we divide the 1D domain into two sub-domains, say liquid and solid. The liquid and solid domains are represented by diffusion equations with different diffusion coefficients. We use explicit finite differences to discretize the diffusion equation. At the interface, we considered one grid point overlap between the subdomains and called it as loose coupling. It is similar to non-overlapping Schwarz method, which is described in the subsection 3.3.1.1. In addition, we also implemented tight coupling where we consider larger overlap between the two subdomains (five grid point). It is similar to overlapping Schwarz method described in subsection 3.3.1.2. However non-overlapping and overlapping Schwarz methods described in Chapter 3 are only for a fixed interface. In our study, as we are dealing with a moving interface, we derived a coupling equation derived based on first principle approach, described in section 3.4.2. In loose coupling, the coupling equation is discretized using single order forward and backward finite difference approximations to compute solid and liquid fluxes respectively. In tight coupling, due to larger overlap, we discretized the coupling equation using second order finite difference approximations for solid and liquid fluxes, thereby new interface temperature is computed. We then considered

Schwarz like iterations to update the boundary conditions at the interface and interpolation to compute the new interface position, described in Chapter 4. The results of loose and tight coupling methods are compared to the numerical solution of Stefan problem. The physical derivation and the mathematical formulation of the Stefan problem is described in Chapter 2.

With the implemented coupling method, we address whether this iterative method could improve the coupling when compared to Stefan problem. The literature [33], [34], [35] showed that the increase of overlap between the subdomains improves the coupling solution, but with a fixed interface. However, in our study, we address if the larger overlap, so called tight coupling could improve the coupling with a moving interface. Moreover, the coupling solution not only depends on the interface conditions but also on the parameters in the coupling equation [10], [11], [36], [37]. Therefore, our study addresses whether the constant parameters of the coupling equation effects the loose and tight coupling solutions. The answers for these questions and conclusions are explained in chapter 4.

<center>**Chapter 2**</center>

<center>**Two Phase Stefan problem**</center>

2.1 1D Diffusion Equation

2.1.1 Introduction

In this chapter, we derive 1D diffusion equation in three different ways in section 2.1.1, 2.1.2, 2.2.1. The diffusion equation is a partial differential equation which describes density fluctuations in a material undergoing diffusion. The equations below are taken from [38]

$$\frac{\partial u(\mathbf{r}, t)}{\partial t} = \nabla \cdot (D(u(\mathbf{r}, t), r)\nabla u(\mathbf{r}, t)). \tag{2.1}$$

where u($\mathbf{r}$,t) is the density of the diffusing material at location r = (x,y,z) at time t. D(u($\mathbf{r}$,t),r) is the diffusion coefficient for density u at location r.

In case if the diffusion coefficient does not depend on density, then the equation (2.1) becomes:

$$\frac{\partial u(\mathbf{r}, t)}{\partial t} = D\nabla^2 u(\mathbf{r}, t)). \tag{2.2}$$

Equation (2.2) also describes the distribution of temperature over time and is called heat equation. The heat equation can be derived from the continuity equation, which states that a change in density in any part of the system is due to inflow and outflow of material into and out of that part of the system. As a result, no matter is created or destroyed.

$$\frac{\partial u}{\partial t} + \nabla \cdot \Gamma = 0 \tag{2.3}$$

where Γ is the flux of the diffusing material. Equation (2.2) can be obtained easily from the last equation when combined with the phenomenological Fick's first law, which assumes that the flux of the diffusing material in any part of the system is proportional to the local density gradient:

$$\Gamma = -D\nabla(u(\mathbf{r}, t)). \tag{2.4}$$

2.1.2 Physical Derivation

In this section, we describe the three physical principles to understand the flow of heat from higher temperature to lower temperature region from the lecture notes of partial differential equations [39].

(1) Heat energy of a body with uniform properties

$$\text{Heat energy} = cmu$$

where m is the body mass, u is the temperature, c is the specific heat which states the amount of heat per unit mass required to raise the temperature by one degree Celsius.

(2) Fourier's law of heat transfer : The law of heat conduction also known as Fourier's law states that the rate of heat transfer through a material is proportional to the negative gradient in the temperature and to the area, at right angles to that gradient, through which the heat flows.

$$\frac{\text{Rate of heat transfer}}{\text{Area}} = -k_0 \frac{\partial u}{\partial x} \tag{2.5}$$

where k_0 is the thermal conductivity, units $[k_0] = MLT^{-3}U^{-1}$.

(3) Conservation of Energy : Consider a rod of length l with non-uniform temperature lying on x-axis from x = 0 to x = l, with constant density ρ, specific heat c, thermal conductivity k_0, cross sectional area A. Consider an arbitrary thin slice of rod of width Δx between x and x+Δx. We consider thin slice so that the temperature throughout the rod remains same i.e, u(x,t). We assume that the sides of the rod are insulated and the ends are only exposed. It is also assumed that there is no heat source within the rod.

$$\text{Heat energy of segment} = c \, \rho \, A \, \Delta x \, u(x, t)$$

By conservation of energy,

Change of heat energy at time Δt = heat in from left boundary – heat out from right boundary

From Fourier's law (2.5),

$$c \, \rho \, A\Delta x u(x, t + \Delta t) - c\rho A\Delta x u(x, t) = \Delta t A\left(-k_0\frac{\partial u}{\partial x}\right)_x - \Delta t A\left(-k_0\frac{\partial u}{\partial x}\right)_{(x+\Delta x)} \quad (2.6)$$

Rearranging (2.6) leads to

$$\frac{u(x, t + \Delta t) - u(x, t)}{\Delta t} = \frac{k_0}{c\rho}\left(\frac{\left(\frac{\partial u}{\partial x}\right)_{(x+\Delta x)} - \left(\frac{\partial u}{\partial x}\right)_x}{\Delta x}\right)$$

Taking the limit Δt, Δx x→0 gives the heat equation

$$\frac{\partial u}{\partial t} = D\frac{\partial^2 u}{\partial x^2} \quad (2.7)$$

where

$$D = \frac{k_0}{c\rho} \quad (2.8)$$

is called thermal diffusivity, units $[k] = L^2$ / T. Since the slice was chosen arbitrarily, the heat equation (2.7) applies throughout the rod.

2.1.3   Analytical Solution

The analytical solution below for the diffusion equation is taken from the literature [39]. Consider the following initial condition

$$u(x, 0) = f(x) \quad \forall \quad x \in [0, L] \tag{2.9}$$

and with boundary conditions

$$u(0, t) = u(L, t) = 0, \quad \forall \quad t > 0. \tag{2.10}$$

Using separation of variables to (2.7) with boundary conditions (2.10), it is attempted here [39] to find a non-trivial solution; i.e

$$u(x, t) = X(x)T(t)$$

Substituting above equation in (2.7), we get

$$\frac{1}{D} \frac{\partial T^{'}(t)}{\partial T(t)} = \frac{\partial X^{''}(x)}{\partial X(x)}$$

Since left hand side depends on t and right hand side depends on x, a constant λ is considered to make both sides equal. Negative sign for λ is used here for convenience.

$$\frac{1}{D} \frac{\partial T^{'}(t)}{\partial T(t)} = \frac{\partial X^{''}(x)}{\partial X(x)} = -\lambda$$

$$X^{''}(x) + \lambda X(x) = 0, \tag{2.11}$$

$$T^{'}(t) + D\lambda T(t) = 0. \tag{2.12}$$

By taking into account, the boundary condition (2.10) for equation (2.11), we get

$$u(0, t) = X(0)T(t) = 0 \implies X(0) = 0,$$

$$u(L, t) = X(L)T(t) = 0 \implies X(L) = 0.$$

The problem of finding the solution for (2.7) reduces to the solving of linear ODE and three different cases are considered with respect to sign of λ.

(1) $\lambda < 0$:

$$X(x) = C_1 e^{\sqrt{-\lambda}x} + C_2 e^{-\sqrt{-\lambda}x}.$$

Taking into boundary condition one gets C_1 and $C_2 = 0$, so for $\lambda < 0$, there exits only trivial solution.

(2) $\lambda = 0$:

$$X(x) = C_1 x + C_2$$

Again, we get only trivial solution for the problem $(C_1 = C_2 = 0)$ due to the boundary conditions.

(3) $\lambda > 0$:

$$X(x) = C_1 \cos(\sqrt{\lambda}x) + C_2 \sin(\sqrt{\lambda}x)$$

Substituting the boundary conditions leads to the following equations for C_1 and C_2.

$$X(0) = C_1 = 0,$$

$$X(L) = C_2 \sin(\sqrt{\lambda}L) = 0 \implies \sin(\sqrt{\lambda}L) = 0, \lambda_n = (\frac{\pi n}{L})^2, n = 1, 2, ...$$

Hence

$$X(t) = C_n \sin\left(\frac{\pi n}{L}x\right)$$

The second equation (2.12) for the function $T(t)$ takes the form :

$$T'(t) + D\left(\frac{\pi n}{L}\right)T(t) = 0 \implies T(t) = B_n \exp\left(-D\left(\frac{\pi n}{L}\right)^2 t\right),$$

where B_n is constant. The general solution for equation (2.7) can be written as :

$$u(x, t) = \sum_{n=1}^{\infty} A_n \sin\left(\frac{\pi n}{L}x\right) \exp\left(-D\left(\frac{\pi n}{L}\right)^2 t\right),$$

where A_n is a constant. We use the initial condition (2.9), to find A_n. If we write the function $f(x)$ as a Fourier series, we obtain :

$$f(x) = \sum_{n=1}^{\infty} F_n \sin\left(\frac{\pi n}{L}x\right) = \sum_{n=1}^{\infty} A_n \sin\left(\frac{\pi n}{L}x\right),$$

$$F_n = A_n = \frac{2}{L} \int_0^L f(\xi) \sin\left(\frac{\pi n}{L}\xi\right) d\xi.$$

Hence the general solution for (2.7) reads:

$$u(x,t) = \sum_{n=1}^{\infty} \left(\frac{2}{L} \int_0^L f(\xi) \sin\left(\frac{\pi n}{L}\xi\right) d\xi\right) \sin\left(\frac{\pi n}{L}x\right) \exp\left(-D\left(\frac{\pi n}{L}\right)^2 t\right)$$

2.2   1D Stefan Problem

2.2.1   Physical Background

A Stefan problem is a specific type of boundary value problem for a differential equation that involves the distribution of heat in a phase changing medium [22], [23], [24], [25],. Some of the examples of Stefan problem are the melting of ice, solidification, fluid flow in porous media, shock waves in gas dynamics [40]. In 1889, Austrian physicist and mathematician Joseph Stefan published a paper [22] describing mathematical models for real physical problems with a change of phase state. When a phase transition occurs(for example change of phase from solid to liquid during melting of ice or liquid to solid during freezing of water), latent heat is either absorbed or released by the thermodynamic system without changing the temperature.

In this section, the equation for the distribution of heat is derived based on the literature [41]. Consider any open and piece-wise smooth region Ω where $\Omega \subset \mathbb{R}^n$, with a boundary $\partial\Omega$. By natural assumption the rate of change of a total quantity should be equal to the net flux through the boundary $\partial\Omega$:

$$\frac{d}{dt} \int_{\Omega} u \, dV = \int_{\partial\Omega} F.\nu \, dS = \int_{\Omega} -\nabla \cdot F \, dV \tag{2.13}$$

where u is the density of some quantity (such as heat), ν being the unit normal pointing inwards and F being the flux density. Gauss theorem is used for the equation (2.13) under the condition that the flux function F defined on the domain Ω is continuously differentiable. Leibniz rule is used for differentiation under the integral sign on the first integral in equation

(2.13), assuming u and u_t exist and are continuous.

$$\int_\Omega \frac{\partial u}{\partial t} dV = \int_\Omega -\nabla \cdot F \, dV \qquad (2.14)$$

Theorem 1 Let f be any function such $f \in C(\Omega)$ where $\Omega \in \mathbb{R}^n$, If $\int_V f \, dV(x) = 0$, for all test volumes $V \subset \Omega$, then $f \equiv 0$ on Ω.

Proof. Assume $f \not\equiv 0$, then at a point $x_0 \in \Omega$, $f(x_0) = \lambda > 0$. But since f is continuous we have for any ε, for instance $\varepsilon = \lambda/2 > 0$, there is a $\delta > 0$ such that if

$$|x - x_0| < \delta, x \in \Omega \Rightarrow |f(x) - f(x_0)| < \varepsilon = \lambda/2$$

which implies that

$$\lambda/2 < f(x) < 3\lambda/2$$

and by integrating the inequality above over the test volume V

$$\int_V f(x) \, dx > \int_V \lambda/2 \, dx = \lambda/2 \times \text{volume}(V) > 0$$

Therefore, we can conclude that

$$\int_V f(x) \, dx > 0.$$

This is a contradiction, thus we have $f \equiv 0$. □

By writing the equation (2.14) as

$$\int_\Omega \frac{\partial u}{\partial t} + \nabla \cdot F \, dV = 0$$

we must conclude from the above theorem that

$$u_t = -\nabla \cdot F. \qquad (2.15)$$

The flux density F is often proportional to the negative gradient of u (minus since the flow is from higher heat to lower heat):

$$F = -\alpha Du (\alpha > 0) \qquad (2.16)$$

where α is the thermal diffusivity. Assuming that α is constant, we get by equation (2.16) and equation (2.15) the heat equation:

$$u_t = \nabla \cdot (Du) = \alpha \Delta u. \tag{2.17}$$

2.2.2 Stefan Condition

The derivation below for the Stefan condition is taken from [41]. However, we do not consider the interface in the shape of disc as mentioned in [41], but in our study, we consider a 1D interface. From the Figure 2.1, consider a domain Ω at a fixed time $t = t_0$ divided into two sub-domains Ω_1 and Ω_2 called as liquid and slid phases respectively. We assume plane symmetry to have the temperature u to depend on only t and x. At $s(t_0)$, the interface divides the two phases. The temperature at the interface $s(t)$ is assumed to be constant at u_m. The movement of the interface $s(t)$ depends on the difference of heat fluxes between the two phases. During the transition, there will be a small volume change, but this property is ignored for simplicity. By physical reason the temperature should be continuous at the interface $x = s(t)$ between the two phases.

$$\lim_{x \to s(t)^+} u_S(x, t) = \lim_{x \to s(t)^-} u_L(x, t) = u_m \quad \text{for all t.} \tag{2.18}$$

Here we consider the melting case., where the interface moves to the right. In such case, it is expected that the temperature is greater than or equal to interface temperature ($u \geq u_m$) in the liquid phase and less than or equal to the interface temperature ($u \leq u_m$) in the solid phase. At time $t = t_0$ consider a interface of area S. Later at time $t_1 > t_0$ the position of the interface has changed to $s(t_1) > s(t_0)$. Consider a volume $S \times (s(t_1) - s(t_0))$ has melted and therefore released a quantity of heat Q.

$$Q = S(s(t_1) - s(t_0)) \times \rho \; H_f \tag{2.19}$$
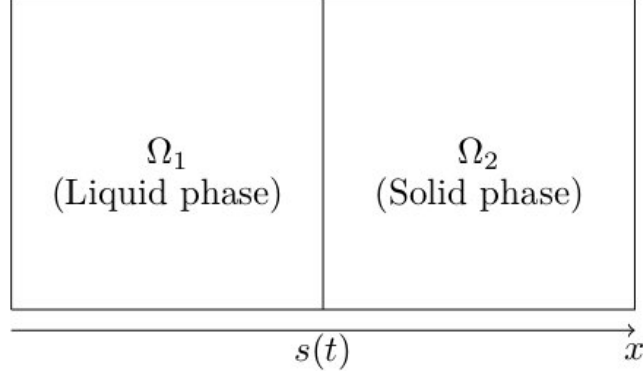
Figure 2.1: Figure is taken from [41]. Domain Ω separated into two phases at x = s(t), which are $\Omega_1 = \Omega \cap x < s(t)$ and $\Omega_2 = \Omega \cap x > s(t)$

where H_f is the specific heat content and ρ is the density. The heat flux for liquid and solid domains respectively are

$$\Phi_l = k_l Du_l \tag{2.20}$$

$$\Phi_s = k_s Du_s \tag{2.21}$$

where k_l and k_s are the conductivity for liquid and solid respectively. By energy conservation it is natural to assume that the total heat absorbed in equation (2.19) is equal to

$$Q = \int_{t_0}^{t_1} [\Phi_l.\hat{x} + \Phi_s.(-\hat{x})]d\tau = \int_{t_0}^{t_1} [-k_l.Du_l(s(\tau), \tau).\hat{x} - k_s.Du_s(s(\tau), \tau).(-\hat{x})] \, d\tau \tag{2.22}$$

where $\hat{x}$ is the unit vector in the x direction. Integrating expression (2.22) over the spatial coordinates gives

$$Q = \int_{t_0}^{t_1} [-k_l \frac{\partial u_l}{\partial x}(s(\tau), \tau) + k_s \frac{\partial u_s}{\partial x}(s(\tau), \tau)] \, d\tau \tag{2.23}$$

we assume this to be equal to expression (2.19). Equating the equations (2.19) and (2.23), we get

$$(s(t_1) - s(t_0)) \, \rho \, H_f = \int_{t_0}^{t_1} [-k_l \frac{\partial u_l}{\partial x}(s(\tau), \tau) + k_s \frac{\partial u_s}{\partial x}(s(\tau), \tau)] \, d\tau \tag{2.24}$$

by dividing with (t_1-t_0) and taking the limit $t_1 \to t_0$, we get

$$\rho \, H_f \lim_{t_1 \to t_0} \frac{s(t_1) - s(t_0)}{(t_1 - t_0)} = \lim_{t_1 \to t_0} \frac{1}{(t_1 - t_0)} \int_{t_0}^{t_1} [-k_l \frac{\partial u_l}{\partial x}(s(\tau), \tau) + k_s \frac{\partial u_s}{\partial x}(s(\tau), \tau)] \, d\tau. \tag{2.25}$$

Theorem 2 (The Intermediate Value Theorem) Let f:[a,b] $\rightarrow$ $\mathbb{R}$ and f $\in$ C, then f attains all values between the end points f(a) and f(b), Proof in [42]

Theorem 3 (The Extreme Value Theorem) A continuous function on a bounded and a closed interval [a,b], attains both a maximum and a minimum value at least once, Proof in [42].

Theorem 4 (Mean Value Theorem) If f : [a,b] $\rightarrow$ $\mathbb{R}$ and f $\in$ C on [a,b], the there exists a number c $\in$ [a,b] such that

$$\int_a^b f(x) \ dx = (b-a) \ f(c) \tag{2.26}$$

From Theorem 3 (Extreme value theorem), we know that a continuous function f(x) has a minimum value m and a maximum value M on a interval [a,b]. From the monotonicity of integrals and m$\leq$f(x)$\leq$M, it follows that

$$mI = \int_a^b mdx \leq \int_a^b f(x)dx \leq \int_a^b Mdx = MI \tag{2.27}$$

where

$$I = \int_a^b dx = b-a \tag{2.28}$$

using (2.28) and dividing by I (assuming I > 0) in equation (2.27) gives

$$m \leq \frac{1}{b-a} \int_a^b f(x)dx \ \leq M \tag{2.29}$$

From Theorem 3, we know that both m and M is attained at least once by the integral. Therefore the Intermediate value theorem says that the function f attains all values in [m,M], more specific it exits a c $\in$ [a,b] such that

$$f(c) = \frac{1}{b-a} \int_a^b f(x)dx. \tag{2.30}$$

With the help of theorem for integrals, we can write equation (2.25) as

$$\rho \ H_f \ s'(t_1) = \lim_{t_1 \rightarrow t_0} \frac{1}{(t_1-t_0)} \times (t_1-t_0) \ f(c) \tag{2.31}$$

where f(c) is a new function we have introduced for simplicity

$$f(c) = -k_l \ u_x(s(c), c) + k_s \ u_x(s(c), c) \qquad (2.32)$$

$c \in [t_0, t_1]$. But as $t_1 \to t_0$ and f is continuous, then

$$\rho \ H_f \ s'(t_1) = f(t_1) \qquad (2.33)$$

However since the same procedure could be done at any time t instead of t_1, we could instead write

$$\rho \ H_f \ s'(t) = f(t)$$

Hence with the expression for f we reach

$$\rho \ H_f \ \frac{ds}{dt} = k_s \ u_x(s(t), t) - k_l \ u_x(s(t), t) \qquad (2.34)$$

which is called the Stefan condition and is a boundary condition for the moving interface.

2.2.3 Mathematical Formulation of the model

The Stefan problem is motivated by physical melting of sea ice and is named after the Austrian physicist Joseph Stefan [22], [40]. We consider a two phase Stefan problem; where the initial phase is solid at a temperature less than melting one. The solid domain is heated from the side and as a result the temperature increases to reach the melting point and then the liquid appears.

We denote the temperature in the point x at time t by u(x,t). s(t) is the point separating the two phases, which determines the position of the interface. The heat transport through the interface causes its displacement.

This problem can be formulated as heat conduction problem and are described by the following equation :

$$\frac{\partial u}{\partial t} = k_l \frac{\partial^2 u}{\partial x^2}, \quad 0 < t < T, \quad 0 < x < s(t) \qquad (2.35)$$

$$\frac{\partial u}{\partial t} = k_s \frac{\partial^2 u}{\partial x^2}, \quad 0 < t < T, \quad x > s(t) \qquad (2.36)$$

$$u(s(t), t) = u_m, \quad \forall \ t > 0, \quad 0 < t < T \tag{2.37}$$

where k_l and k_s are assumed to constant in time and position. The interface temperature u_m is assumed to be constant.

The position of the interface is determined by the jump condition also called Stefan condition, it represent the energy conservation on the interface. Stefan condition is described by the following equation :

$$\rho \ H_f \ \frac{ds}{dt} = k_s \ \frac{\partial u}{\partial x}\big|_{x>s(t)} - k_l \ \frac{\partial u}{\partial x}\big|_{x<s(t)}, \tag{2.38}$$

where H_f and ρ are assumed to be constant.

$$u(x, 0) = u_s < u_m, \quad 0 < x \leq X \tag{2.39}$$

$$s(0) = 0 \tag{2.40}$$

$$u(0, t) = u_l > u_m, \quad \forall \ t > 0, \quad 0 < t < T \tag{2.41}$$

$$u(X, t) = u_s < u_m, \quad \forall \ t > 0, \quad 0 < t < T \tag{2.42}$$

equations (2.39) and (2.40) are the initial conditions and equations (2.41) and (2.42) are the constant boundary conditions for the domain.

2.2.4   Similarity Solution

Figure 2.2 represents the Similarity solution (analytical solution) of the Stefan problem. The derivation of the similarity solution for the Stefan problem is given by [41]. A similarity ξ is introduced, which is defined by :

$$\xi = \frac{x}{\sqrt{t}} \tag{2.43}$$

and thus seeks the solution of function

$$u(x, t) = F(\xi(x, t)) \tag{2.44}$$

where $F(\xi)$ is an unknown function, yet to be found. Substituting (2.44) in (2.35) we get,

$$\frac{\partial u(x, t)}{\partial t} = \frac{dF}{d\xi} \frac{\partial \xi}{\partial t} = \frac{-x}{2t\sqrt{t}} \frac{dF}{d\xi}, \tag{2.45}$$

$$\frac{\partial u(x,t)}{\partial x} = \frac{dF}{d\xi}\frac{\partial \xi}{\partial x} = \frac{-1}{\sqrt{t}}\frac{dF}{d\xi}, \tag{2.46}$$

$$k_l\frac{\partial u^2(x,t)}{\partial x^2} = k_l\frac{1}{\sqrt{t}}\frac{d}{d\xi}\left(\frac{dF}{d\xi}\right)\frac{\partial \xi}{\partial x} = k_l\frac{1}{t}\frac{d^2F}{d\xi^2} \tag{2.47}$$

Equations (2.45) and (2.47) gives the second order linear homogeneous differential equation.

$$\frac{d^2F}{d\xi^2} + \frac{\xi}{2k_l}\frac{dF}{d\xi} = 0 \tag{2.48}$$

which can be solved with an integrating factor

$$M(\xi) = e^{\int_{s_0}^{\xi} \frac{s}{2k_l}ds} = C_1 e^{\frac{\xi^2}{4k_l}} \tag{2.49}$$

where C_1 is an integration constant. $M(x)$ in Equation (2.49) is multiplied with (2.48) and by the product rule we get,

$$\frac{d^2F}{d\xi}M(\xi + \frac{\xi}{2k_l}M(\xi)\frac{dF}{d\xi} = \frac{d}{d\xi}(M(\xi)\frac{dF}{d\xi}) = 0 \tag{2.50}$$

and by integrating (2.50) we get

$$M(\xi)\frac{dF}{d\xi} = C_2 \tag{2.51}$$

where C_2 is an integration constant. From the fundamental theorem of calculus the solution of equation (2.51) is

$$F(\xi) = C\int_0^{\xi} e^{\frac{-s^2}{4k_l}}ds + D \tag{2.52}$$

where D is an integration constant. By substituting $y = \frac{s}{\sqrt{2k_l}}$, Equation (2.52) could be written in terms of error function.

$$F(\xi) = A\text{erf}(\frac{\xi}{2\sqrt{k_l}} + D \tag{2.53}$$

and thus the solution to (2.35) is

$$u(x,t) = F(\frac{x}{\sqrt{t}}) = A\text{erf}(\frac{x}{2\sqrt{tk_l}}) + D \tag{2.54}$$

From the boundary condition $x = 0$ and $x = s(t)$, we get

$$D = u_0 \tag{2.55}$$

and

$$A = \frac{0 - u_0}{\mathrm{erf}(\lambda)} \tag{2.56}$$

where

$$\lambda \equiv \frac{s(t)}{2\sqrt{tk_l}} \tag{2.57}$$

Since A in equation (2.56) is constant, it follows that λ is also constant thus

$$s(t) = 2\lambda\sqrt{tk_l} \tag{2.58}$$

with the constants A and D, the solution is

$$u(x,t) = u_0 - \frac{u_0}{\mathrm{erf}(\lambda)}\mathrm{erf}(\frac{x}{2\sqrt{k_l t}}) \tag{2.59}$$

About the parameter λ:

The Stefan condition at the free boundary $x = s(t)$ is

$$\rho \, H_f \, \frac{ds}{dt} = -k_l \, u_x(s(t), t) \tag{2.60}$$

and the time derivative of $s(t)$ is

$$\frac{ds}{dt} = \frac{d}{dt}(2\lambda\sqrt{k_l \, t}) = \lambda\frac{\sqrt{k_l}}{\sqrt{t}} \tag{2.61}$$

and for the other derivative in the Stefan condition, we need to take the spatial derivative of the solution u, given by (2.59)

$$u_x(x,t) = -\frac{u_0}{\mathrm{erf}(\lambda)} \, \frac{2}{\sqrt{\pi}} \, \frac{d}{dx}\int_0^{\frac{x}{2\sqrt{k_l t}}} e^{(-y^2)}dy = -\frac{u_0}{\mathrm{erf}(\lambda)} \, \frac{1}{\sqrt{\pi}} \frac{e^{\frac{-x^2}{4k_l t}}}{\sqrt{k_l t}} \tag{2.62}$$

and at $x = s(t)$

$$u_x(s(t), t) = -\frac{u_0}{\mathrm{erf}(\lambda)} \frac{e^{-\lambda^2}}{\sqrt{k_l t}\sqrt{\pi}} \tag{2.63}$$

By putting the equations (2.63) and (2.61) in the Stefan condition (2.60) and solving for λ, we get the following transcendental equation.

$$\lambda e^{\lambda^2} \, \mathrm{erf}(\lambda) = \frac{St_l}{\sqrt{\pi}} \tag{2.64}$$

where St_l is the Stefan number in [24]

Summing up the solution of u(x,t) and s(t), and the condition for λ, gives

$$\begin{cases} u(x,t) = u_0 - \dfrac{u_o}{\text{erf}(\lambda)} \ \text{erf}(\dfrac{x}{2\sqrt{k_l \ t}}) \\[3ex] s(t) = 2\lambda \ \sqrt{k_l t} \\[3ex] \lambda \ e^{\lambda 2} \ \text{erf}(\lambda) = \dfrac{St_l}{\sqrt{\pi}} \end{cases}$$

The above solution can be derived only for certain parameters. As a result, we do not consider the above solution of Stefan problem as the reference. We compare the solution of coupling methods with a numerical solution of Stefan problem.

2.3   Discretization

2.3.1   Explicit method

We discretize the diffusion equation using forward in time and centred difference in space. Let ib is the index at the interface. The numerical algorithm for diffusion equation (2.35) in liquid domain:

$$\frac{(u_i^{n+1} - u_i^n)}{\Delta t} = \frac{k_l}{(\Delta x)^2}(u_{i+1}^n - 2u_i^n + u_{i-1}^n) \tag{2.65}$$

The numerical algorithm for diffusion equation (2.36) in solid domain is:

$$\frac{(u_i^{n+1} - u_i^n)}{\Delta t} = \frac{k_s}{(\Delta x)^2}(u_{i+1}^n - 2u_i^n + u_{i-1}^n) \tag{2.66}$$

The numerical algorithm for the Stefan condition ((2.38)) to compute the change in interface is:

$$\rho H_f \frac{(s^{n+1} - s^n)}{\Delta t} = \frac{k_s}{\Delta x}(u_{ib+1}^n - u_{ib}^n) - \frac{k_l}{\Delta x}(u_{ib}^n - u_{ib-1}^n) \tag{2.67}$$

where $\frac{k_s}{\Delta x} \ (u_{ib+1}^n - u_{ib}^n)$ and $\frac{k_l}{\Delta x} \ (u_{ib}^n - u_{ib-1}^n)$ are discretized using forward and backward finite difference method, representing solid and liquid flux respectively.
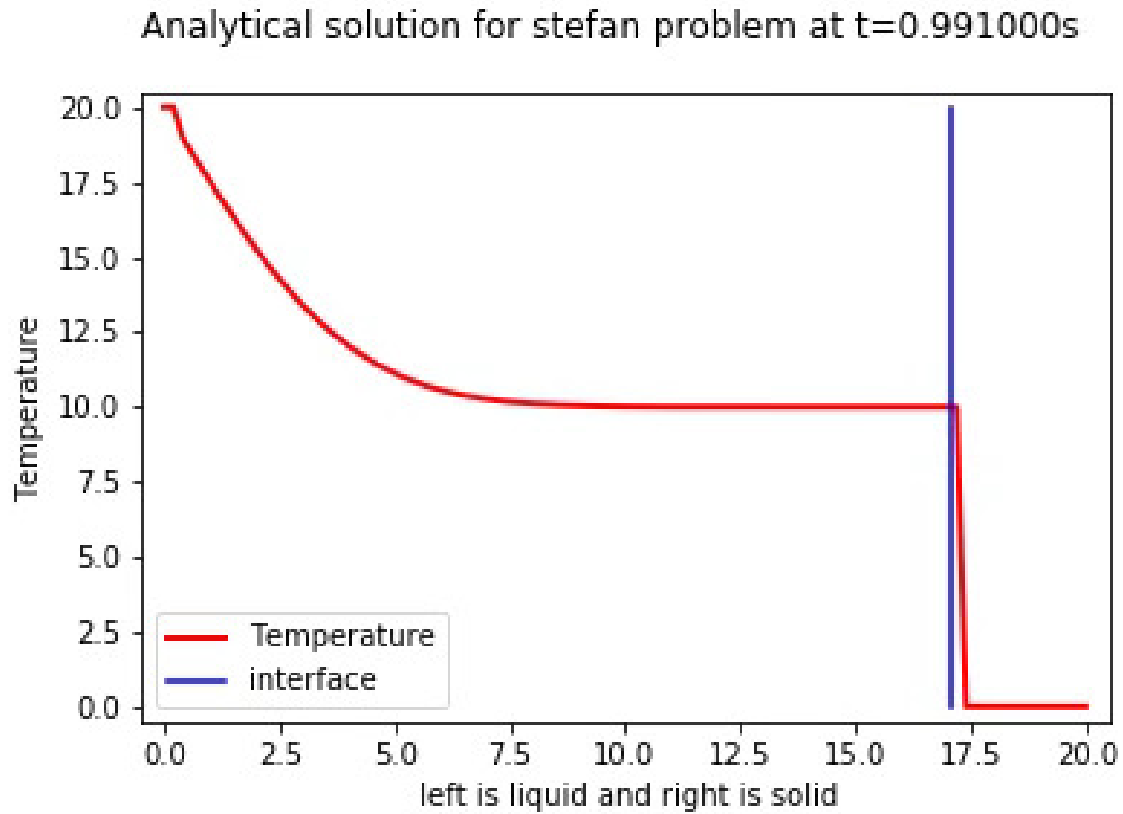
Figure 2.2: represents analytical solution for the Stefan problem. Red line represents diffusion of temperature and blue line s(t) represents the position of interface. x axis denotes the domain, where left of s(t) is liquid and the right is solid. y axis denotes the temperature

.
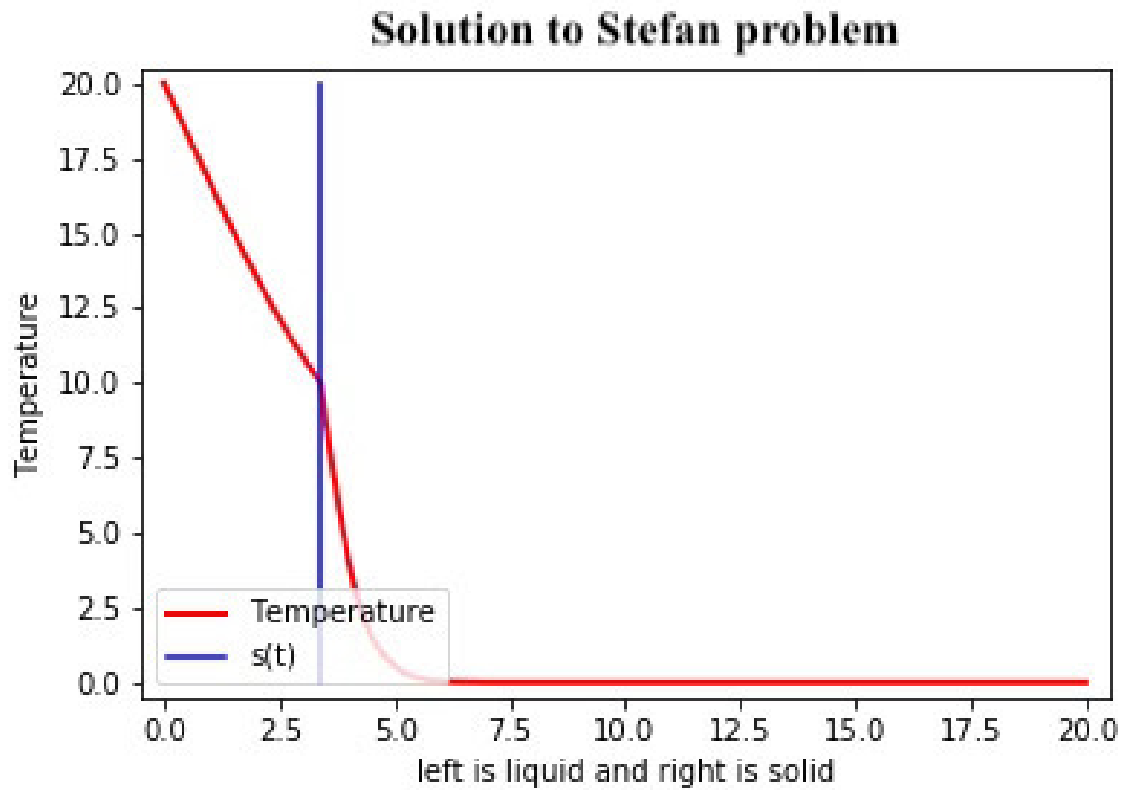
Figure 2.3: Discretization of Stefan problem using explicit method. Red line represents diffusion of temperature and blue line s(t) represents the position of interface. x axis denotes the domain, where left of s(t) is liquid and the right is solid and y axis denotes the temperature

2.3.2   Implicit method

Here we discretize the diffusion equation and Stefan condition using implicit method in order to avoid instability in the explicit method. The principal reason for using implicit solution methods, which are more complex to program and require more computational effort in each solution step, is to allow for large time-step sizes.

However, in our study, we do not use implicit method as our interest is not to run our model for long time steps, but to understand the loose and tight coupling methods with a moving interface using Schwarz iterations. Therefore we use only explicit method to discretize Stefan problem and coupling methods.

The numerical algorithm for heat equation in liquid region is

$$\frac{(u_i^{n+1} - u_i^n)}{\Delta t} = \frac{k_l}{(\Delta x)^2}(u_{i+1}^{n+1} - 2u_i^{n+1} + u_{i-1}^{n+1}) \tag{2.68}$$

The corresponding numerical algorithm for heat equation in solid is

$$\frac{(u_i^{n+1} - u_i^n)}{\Delta t} = \frac{k_s}{(\Delta x)^2}(u_{i+1}^{n+1} - 2u_i^{n+1} + u_{i-1}^{n+1}) \tag{2.69}$$

The numerical algorithm for Stefan condition

$$\rho H_f \frac{(s^{n+1} - s^n)}{\Delta t} = \frac{k_s}{\Delta x}(u_{ib+1}^n - u_{ib}^n) - \frac{k_l}{\Delta x}(u_{ib}^{n+1} - u_{ib-1}^{n+1}) \tag{2.70}$$

Now, in chapter 3, we discuss the loose and tight coupling methods similar to non-overlapping and overlapping Schwarz method respectively. However, these Schwarz methods [10], [11] described in 3.3 are for a fixed interface, therefore in section 3.4.2 we derived the coupling equation (3.15) for the moving interface. The results comparing these coupling method with Stefan problem (in chapter 2) are further explained in chapter 4.

Chapter 3

Coupling Strategies

3.1   Introduction

The interaction of sea ice with ocean and atmosphere is one of the important interactions among the models represent [43], [4], [44], [45]. This is because the sea ice forms an interface between ocean and atmosphere and is responsible for exchange of heat, moisture and momentum between them [43], [46], [47], [48]. The factors that effect sea-ice by thermal processes are downward radiation, turbulent heat flux from the atmosphere, the oceanic heat flux from below and by the dynamical processes are wind stress, ocean ice stress and internal ice stress. The relationship between sea ice melt and the heat supplied to the upper ocean from the atmosphere is explained in [49]. It also explains that during the ice melt season, the upper ocean and sea ice are strongly coupled thermodynamically. In addition, the growth and decay of sea ice affects the global thermohaline circulation and the intensity of oceanic deep convection [50].

The study of sea-ice thermodynamics was started by classical Stefan problem (explained in Chapter 2) and the studies continued [51], [52], [53], [13], [54], [55], [56] are useful to understand ice-ocean interactions, ice growth and meting, and mechanism of heat exchange between ocean-ice. Some of the thermodynamic sea-ice models are further summarised in [57]. Various numerical methods (say., explicit, implicit, semi-implicit) are used to discretize the thermal interaction between ocean and ice models by exchanging temperature values and heat fluxes at the fixed interface between them [58] and the stability of these
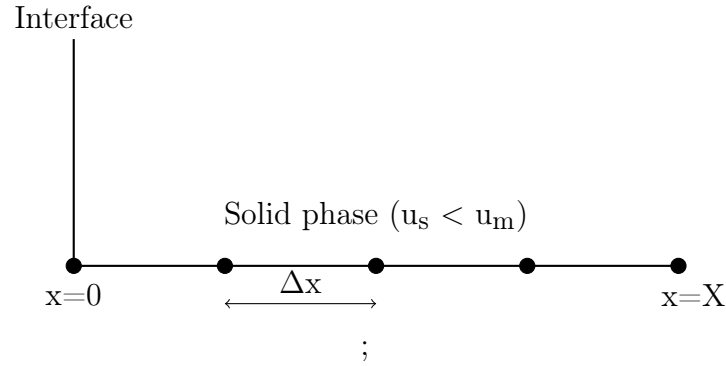
Figure 3.1: Stefan problem and Coupling strategies at t=0

methods are explained in [59] and [60]. These studies to couple ocean and ice subdomains are applied only for a fixed interface between them. But in our study, we implement a moving interface between the two subdomains which is a more "realistic" case. Therefore, in this chapter, we derive the coupling equation(3.15) in section 3.4 at the interface based on first principle approach and implemented loose and tight coupling methods based on non-overlapping and overlapping Schwarz methods respectively. The results of these coupling methods are compared to the Stefan problem discussed in chapter 4.

3.2   Description of the model setup

Figure 3.1 shows the initial condition of the model, where the material is solid and the interface is x = 0. Figure 3.2 represents the movement of the interface based on new interface temperature. We impose a liquid temperature u_l which is greater than melting temperature u_m at x = 0. This results in an increase of temperature from the side x = 0, and when the temperature reaches the melting point, the material starts melting into liquid. The interface separates the two phases, where there is an exchange of temperature values and heat fluxes between the liquid and solid domains.

We consider the same heat equations for liquid and solid domains as in (2.35) and (2.36) respectively, but the interface condition in these coupling methods is different from Stefan's condition (2.38). For simplicity, the interface temperature in a Stefan problem is assumed to
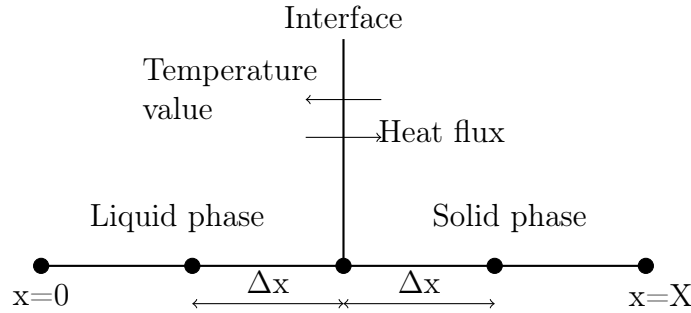
Figure 3.2: Stefan problem and Coupling strategies at t>0.

be constant. We, on the other hand, implement loose and tight coupling methods in which we compute the temperature at the interface using the coupling equation (3.15) derived in section 3.4. In loose coupling, the coupling equation is discretized using low order finite difference method, whereas in tight coupling, higher order finite difference is used to discretize the coupling equation. The solutions to loose and tight coupling methods are compared to the numerical solution of Stefan problem. In the following sections, we elaborate on the implementation of loose and tight coupling methods.

3.3   Description of Schwarz iterative coupling

3.3.1   Schwarz method

Originally Schwarz methods are applied for stationary problems but now widely used for time dependent problems [13]. The idea of Schwarz methods is to separate the whole domain into two sub-domains, which are solved separately. An iteration process is then applied to achieve convergence to the solution of original problem. The drawback of this approach is its iterative nature, which increases the cost of coupling, especially when the convergence is slow.

Schwarz method explained in chapter 1 is for atmosphere-ocean coupling [9], however this numerical model is complex to understand. As a result, in this section we describe Schwarz methods based on [10], [11], applied to a simple one dimensional diffusion equation.

The description of the domain and the equations below are taken from [10]. Consider a one
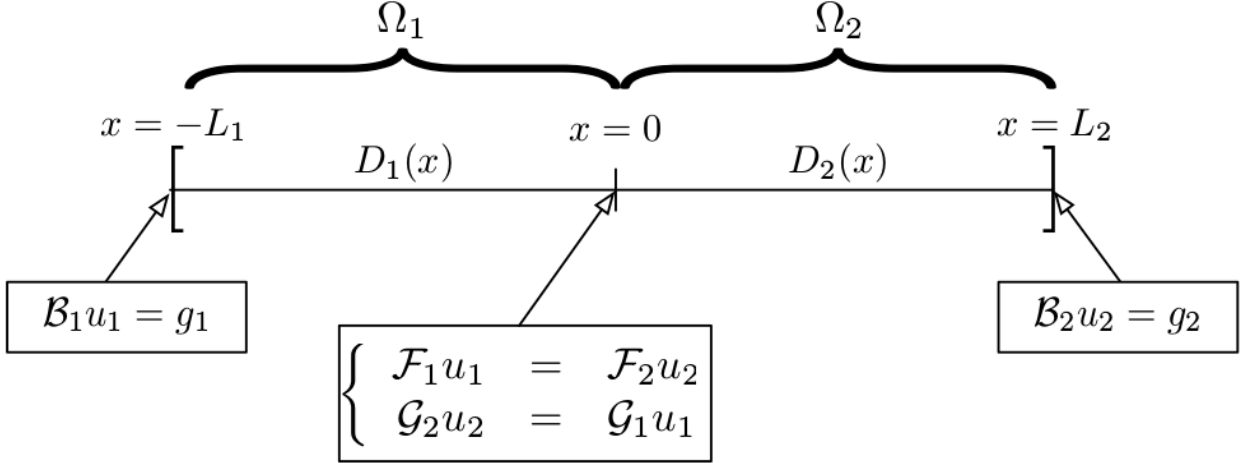
Figure 3.3: Figure is taken from [10]. Decomposition of spatial domain Ω into two non-overlapping subdomains

dimensional diffusion equation in a bounded domain Ω, where $\Omega =]L_1,\ L_2[,(L_1,L_2 \in \mathbb{R}^+)$ with a diffusion coefficient $D(x) > 0$, $x \in \Omega$. Let the diffusion equation be

$$\mathcal{L}u = \partial_t u - \partial_x(D(x)\partial_x u) = f \quad \text{in } \Omega \times [0, T], \tag{3.1}$$

The initial and boundary conditions respectively are:

$$u(x, 0) = u_0(x) \quad x \in \Omega, \tag{3.2}$$

$$\mathcal{B}_1 u(-L_1, t) = g_1 \quad \mathcal{B}_2 u(L_2, t) = g_2 \quad t \in [0, T], \tag{3.3}$$

where $\mathcal{B}_1$ and $\mathcal{B}_2$ are two partial operators.

In order to apply Schwarz method, the domain Ω is divided into two non-overlapping domains Ω_1 and Ω_2 (Figure 3.3). Each subdomain having its own diffusion coefficients $D_j(x)$, $(j = 1,2)$. These subdomains communicate through their common interface $\Gamma = x = 0$. A non-overlapping global-in-time Schwarz algorithm is used to solve the corresponding coupling problem [10], explained further in 3.3.1.1. This method consists in solving iteratively sub problems in $\Omega_1 \times [0,\ T]$ and $\Omega_2 \times [0,\ T]$ using as an interface condition at $x = 0$ the values computed at the previous iteration in the other subdomain.

3.3.1.1   Non overlapping Schwarz method

Consider a operator $\mathcal{L}$ is split into two operators $\mathcal{L}_j = \partial_t - \partial_x(D_j(x)\,\partial_x)$ restricted to Ω_j (j = 1, 2). Introducing the operators $\mathcal{F}_1$, $\mathcal{F}_2$, $\mathcal{G}_1$ and $\mathcal{G}_2$ to define the interface conditions, the algorithm below is taken from [10]:

$$\mathcal{L}_1 u_1^k = f \quad \text{in} \quad \Omega_1 \times [0, T] \tag{3.4}$$

$$u_1^k(x, 0) = u_o(x) \quad x \in \Omega_1 \tag{3.5}$$

$$\mathcal{B}_1 u_1^k(-L_1, t) = g_1, \quad t \in [0, T] \tag{3.6}$$

$$\mathcal{F}_1 u_1^k(0, t) = \mathcal{F}_2 u_2^{k-1}(0, t) \quad \text{in} \quad \Gamma \times [0, T], \tag{3.7}$$

$$\mathcal{L}_2 u_2^k = f \quad \text{in} \quad \Omega_2 \times [0, T] \tag{3.8}$$

$$u_2^k(x, 0) = u_o(x) \quad x \in \Omega_2 \tag{3.9}$$

$$\mathcal{B}_2 u_2^k(L_2, t) = g_2, \quad t \in [0, T] \tag{3.10}$$

$$\mathcal{G}_2 u_2^k(0, t) = \mathcal{G}_1 u_1^k(0, t) \quad \text{in} \quad \Gamma \times [0, T], \tag{3.11}$$

where k = 1,2,.. is the iteration number and where the initial guess $u_2^0(0, t)$ is given. The algorithm (3.4 - 3.11) is called the multiplicative form of the Schwarz method. The loose coupling method, described in section 3.4.3 is similar to the non overlapping method, as there is one grid point overlap between the two sub-domains. However, the method described in this section is basically for a non-moving interface and Dirichlet boundary conditions. We had the problem, that we needed to deal with fluxes over a moving boundary and therefore we changed this scheme in our study.

3.3.1.2   Overlapping Schwarz method

The overlapping of adjacent subdomains Ω_1, and Ω_2 is performed on the region Ω_{12} and Ω_{21} (Figure 3.4) and then a Schwarz alternating procedure or similar algorithms can be applied [33], [35]. Starting with an initial guess in one subdomain (say Ω_1), the computed

.
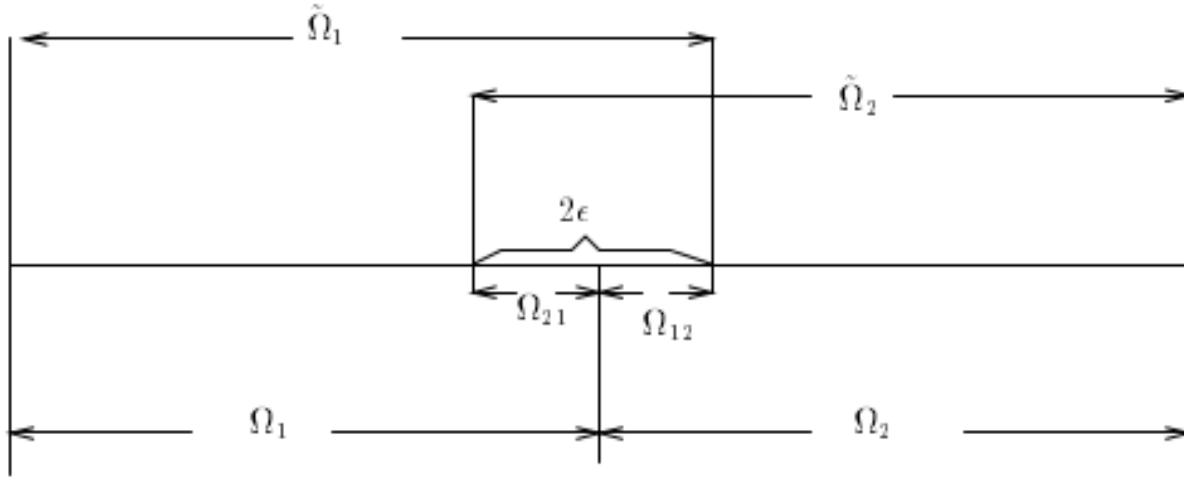
Figure 3.4: The above Figure is taken from [33]. Splitting the domain into Overlapping subdomains

field variables are used to supply the required boundary conditions for the neighbouring (overlapped) subdomain Ω_2. Alternatively, the solution constructed in Ω_2, is employed to update the boundary conditions in Ω_1. The overall iteration is then repeated until convergence. In the case of more than two subdomains they can be implemented in such a way that half of them are treated in parallel. The convergence of Schwarz alternating algorithm has been proven for the model Laplace equation [61] and for nonlinear elliptic equations in [62]. The convergence rate of the Schwarz algorithm improves exponentially with the overlapping size [33], [34], [63],[35].

The tight coupling method, described in section 3.4.4 is similar to the overlapping method, but with a moving boundary at the interface of two subdomains.

3.4   Coupling methods

3.4.1   Introduction

As a preliminary study, we considered a interface condition (B.1) from the literature[58]. This equation (B.1) computes the temperature at the interface based on exchanging fluxes at the interface. However, this equation (B.1) from [58] is used to compute interface temper-

ature for the case of fixed interface. Our problem deals with moving interface and therefore, we derived a coupling equation (3.15) based on first principle approach, where interface temperature is computed for a moving interface. Moreover, in the following sections, we elaborate the further improvements like Schwarz iterations in section 3.3.1 to update the boundary conditions at the interface and interpolation in section 3.4.5 to compute the new interface position. We consider linear interpolation for loose coupling and higher order interpolation for tight coupling to compute the new interface position.

We now apply a logic for implementing coupling methods which is different from the Stefan problem (reference). The two sub-domains, liquid and solid are represented by independent solvers, which communicate by exchanging boundary conditions at the interface. At the interface, we consider one grid point overlap between the sub-domains and called it as loose coupling. It is similar to non - overlapping Schwarz method, which is described in section 3.3.1.1. Loose coupling is widely used in coupling these days to couple various sub components in climate models, for which they use a coupler. This coupler exchanges the averaged fluxes at the boundary layer (one grid point). However, the method is different as our study is focused on moving boundary at the interface. In addition, for tight coupling, we consider five grid point overlap between the sub-domains in order to increase the overlap region at the interface. It is similar to overlapping Schwarz method described in 3.3.1.2, but for a moving interface.

Initially, only one grid point is liquid, and the other nx-1 grid points are considered to be solid. The interface and its position needs to be determined as a diagnostic property after solving the two independent problems and applying some physically meaningful exchange mechanism. We consider Schwarz like iterations to update the boundary conditions at the interface and interpolation to compute the new interface position. In the following sections, we derive the coupling equation to compute the interface temperature, and thereby using low and higher order finite difference methods to discretize the coupling equation for loose and tight coupling methods respectively.

3.4.2   Derivation of Coupling equation

The coupling equation for loose and tight coupling methods described in this section is based on first principle approach. We assume that at any fixed time there is an interface between the solid and the liquid phase of area A. Then we consider that the total energy flux Q through that interface equals

$$Q = A \cdot \rho \; H_f \tag{3.12}$$

Where ρ is the density of the fluid (in our case we assume it to be normalized to $\rho = 1$) and H_f is the latent heat, which is considered to be constant. A is the area of the interface, in 1D it is normalised to 1. With the same nomenclature described in Chapter 2 and 3, we also assume that the heat fluxes out of each of the solid and liquid domains can be described by

$$f_s = k_s \cdot \frac{\partial u_s}{\partial x}, \quad f_l = k_l \cdot \frac{\partial u_l}{\partial x},$$

Now, at any fixed time, the heat flux Q through the interface between the liquid and the solid phase is given by the area integral

$$Q = \int_A \left[-f_l \cdot \hat{x} - f_s \cdot (-\hat{x}) \right] dA.$$

where $\hat{x}$ is the unit vector in the x direction. By energy conservation, we assume that the total heat absorbed in equation (3.12) is equal to

$$Q = A \cdot \rho H_f = \int_A \left[-f_l \cdot \hat{x} - f_s \cdot (-\hat{x}) \right] dA \tag{3.13}$$

$$= - \int_A k_l \frac{\partial u_l}{\partial x} \cdot \hat{x} \; dA + \int_A k_s \frac{\partial u_s}{\partial x} \cdot \hat{x} \; dA \tag{3.14}$$

Since we consider the function u is uniform throughout the area A, equation (3.14) can be written as

$$\rho H_f = -k_l \frac{\partial u_l}{\partial x} + k_s \frac{\partial u_s}{\partial x} \tag{3.15}$$

3.4.3   Algorithm for loose coupling

In loose coupling, we discretize the equation (3.15) by using single order forward and backward finite difference approximation to obtain the new temperature at the interface.

$$\Delta x \; \rho \; H_f + k_l[u_l(i) - u_l(i-1)] = k_s[u_s(i+1) - u_s(i)]$$

$$\Rightarrow \quad \Delta x \; \rho \; H_f + k_l u_l(i) + k_s u_s(i) = k_l u_l(i-1) + k_s u_s(i+1).$$

Since we know – from continuity considerations – that at the interface i we have $u_l(i) = u_s(i) =: \bar{u}$, we can now use as the new interface temperature

$$\bar{u} = \frac{k_s u_s(i+1) + k_l u_l(i-1) - \rho \; H_f \; \Delta x}{k_l + k_s} \tag{3.16}$$

3.4.4   Algorithm for tight coupling

In tight coupling, we discretize the coupling equation (3.15) by using second order finite difference approximations to first order derivatives for liquid and solid fluxes.

for liquid domain(left) :

$$\frac{\partial u_l}{\partial x} = \frac{1}{2\Delta x}[3u_l(i) - 4u_l(i-1) + u_l(i-2)]$$

for solid domain(right) :

$$\frac{\partial u_s}{\partial x} = \frac{1}{2\Delta x}[-3u_s(i) - 4u_s(i+1) - u_s(i+2)]$$

Now, by replacing $\frac{\partial u_l}{\partial x}$ and $\frac{\partial u_s}{\partial x}$ in (3.15), to obtain the new interface temperature

$$2 \; \Delta x \; \rho \; H_f = -3[k_s u_s(i) + k_l u_l(i)] + 4k_s u_s(i+1) - k_s u_s(i+2) + u k_l u_l(i-1) - k_l u_l(i-2)$$

$$2 \; \Delta x \; \rho \; H_f + 3[k_s u_s(i) + k_l u_l(i)] + 4k_s u_s(i+1) - k_s u_s(i+2) + u k_l u_l(i-1) - k_l u_l(i-2)$$

Since we know – from continuity considerations – that at the interface i we have $u_l(i) = u_s(i) =: \bar{u}$, we can now use as the new interface temperature

$$\bar{u} = \frac{k_s[4u_s(i+1) - u_s(i+2)] + k_l[4u_l(i-1) - u_l(i-2)] - 2\Delta x \; \rho \; H_f}{3[k_l + k_s]} \tag{3.17}$$

In further sections, we describe the interpolation to compute the new interface position. We considered linear and higher order interpolation for loose and tight coupling respectively.

3.4.5   Interpolation

Interpolation is explained in this subsection based on the literature [64]. Consider a unknown function $f(x)$ for which there are values at $(n+1)$ distinct points $x_0 < x_1 < ... < x_n$, i.e., $f(x_0), . . . , f(x_n)$ are given. The interpolation problem is to construct a function $Q(x)$ that passes through these points, i.e., to find a function $Q(x)$ such that $Q(x_j) = f(x_j)$, $0 \leq j \leq n$ are satisfied. For example, consider (Figure 3.5) the values of a function that are prescribed at two points: $(x_0, f(x_0))$ and $(x_1, f(x_1))$. There are infinitely many functions that pass through these two points. However, if we limit ourselves to polynomials of degree less than or equal to one, there is only one such function that passes through these two points, it is the line that connects them. A line, in general, is a polynomial of degree one, but if the two given values are equal, $f(x_0) = f(x_1)$, the line that connects them is the constant $Q_0(x) \equiv f(x_0)$, which is a polynomial of degree zero.

In the next subsections 3.4.5.1 and 3.4.5.2, we explain linear and higher order polynomial interpolation. In loose and tight coupling methods, we use linear and higher order interpolation respectively to determine the new position of the interface.

3.4.5.1   Linear Interpolation

From the Figure 3.6, we consider two known grid points (x_0, y_0), (x_1, y_1) , the distance between these grid points is called the linear interpolate. For a value x in the interval (x_0, x_1), the value y along the straight line is given from the equation of slopes

$$\frac{y - y_0}{x - x_0} = \frac{y_1 - y_0}{x_1 - x_0} \tag{3.18}$$

We solve the above equation for y, which is the unknown value at x, gives

$$y = y_0 + (x - x_0)\frac{y_1 - y_0}{x_1 - x_0} \tag{3.19}$$
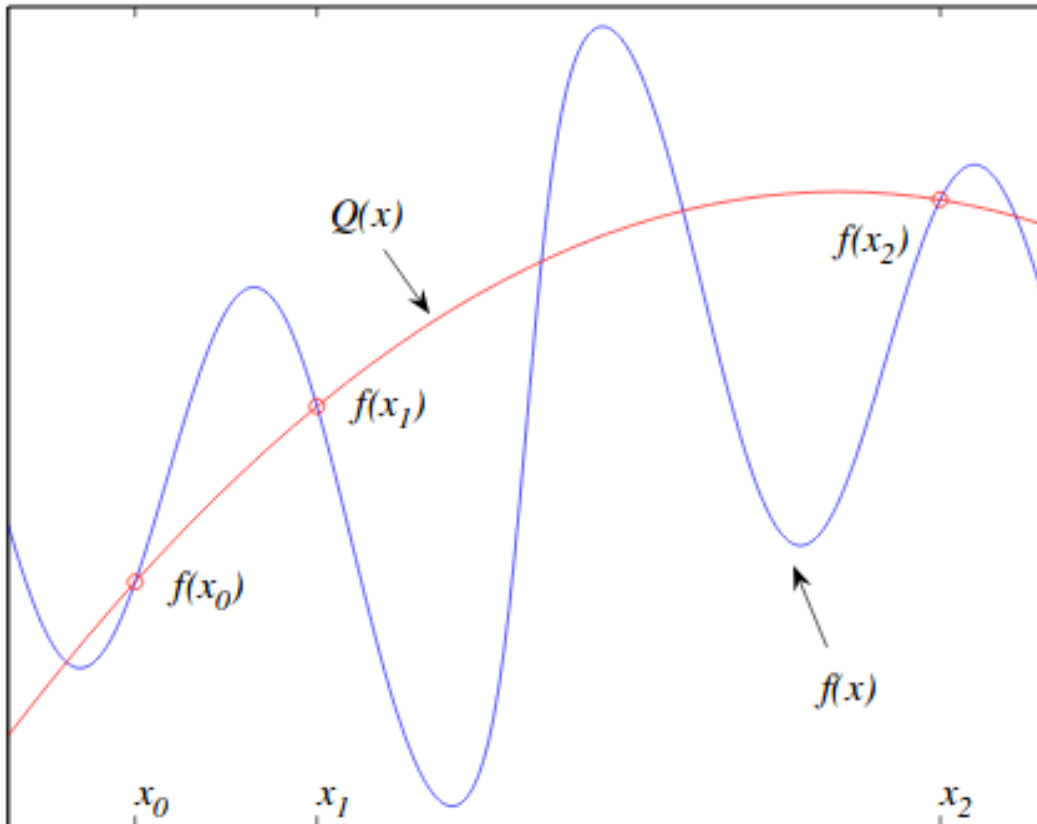
Figure 3.5: The above figure is taken from [64]. The function f(x), the interpolation points x_0, x_1, x_2 and the interpolating polynomial Q(x)

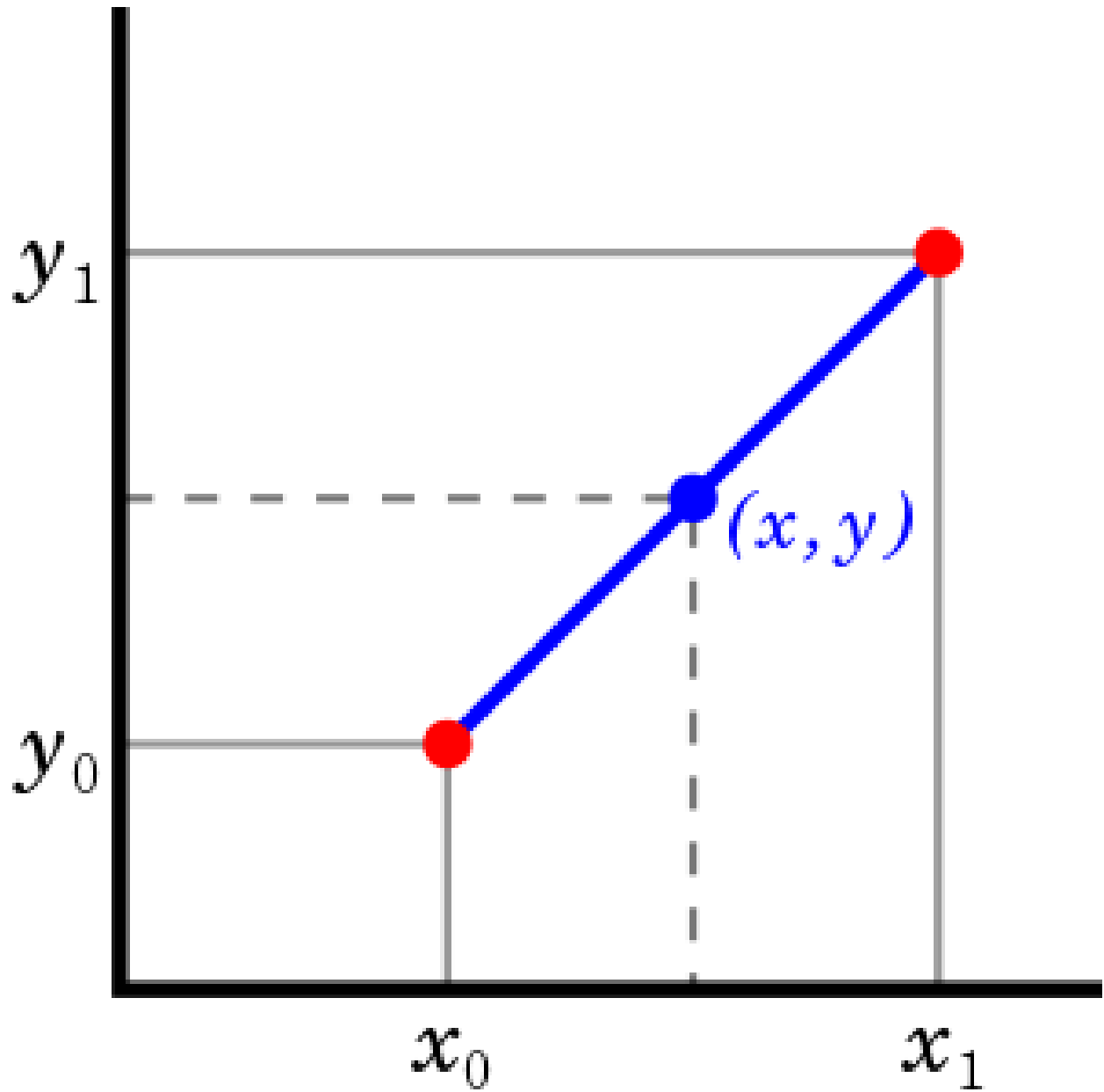Figure 3.6: The figure is taken from [65]. Given the two red points, the blue line is the linear interpolation between the points, and the value y at x may be found by linear interpolation

It is the formula for linear interpolation in the interval (x_0, x_1). Now, let us consider the two known points as (ip, u_{ip}) and (ip+1, u_{ip+1}), where ip and ip+1 are the left and right grid points of interface position, and u_{ip}, u_{ip+1} are temperatures at ip and ip+1 respectively. We assume the temperature in between these grid points ip and ip+1 as melting temperature u_m. Now, in loose coupling, we compute the position of the interface at temperature u_m using linear interpolation.

3.4.5.2   Higher order Interpolation

We use fifth degree polynomial interpolation for tight coupling, as we consider five overlapping grid points between the two domains. Consider a interpolating polynomial P(x) of degree $\leq$ (n-1) that passes through n points $(x_1, y_1 = f(x_1))$, $(x_2, y_2 = f(x_2))$, ..., $(x_n, y_n = f(x_n))$, and is given by

$$P(x) = \sum_{j=1}^{n} P_j(x) \tag{3.20}$$

where

$$P_j(x) = y_j \prod_{k=1, k \neq j}^{n} \frac{x - x_k}{x_j - x_k} \tag{3.21}$$

By writing it explicitly we get

$$P(x) = \frac{(x - x_2)(x - x_3)...(x - x_n)}{(x_1 - x_2)(x_1 - x_3)...(x_1 - x_n)} y_1 + \frac{(x - x_1)(x - x_3)...(x - x_n)}{(x_2 - x_1)(x_2 - x_3)...(x_2 - x_n)} y_2 + ... \tag{3.22}$$

$$... + \frac{(x - x_1)(x - x_2)...(x - x_n)}{(x_1 - x_2)(x_1 - x_3)...(x_1 - x_n)} y_n$$

In tight coupling, we consider higher order polynomial to compute the new interface position. Let us consider five overlapping points (ip-2, u_{ip-2}), (ip-1, u_{ip-1}), (ip, u_{ip}), (ip+1, u_{ip+1}), (ip+2, u_{ip+2}) where u_{ip-2}, u_{ip-1}, u_{ip}, u_{ip+1} and u_{ip+2} are temperatures at ip-2, ip-1, ip, ip+1 and ip+2 grid points respectively. Also consider that the interface position is passing through these points and the temperature at the interface position u_{ip} is assumed to be equal to melting temperature(u_m). Now, by using fifth order interpolation, we compute new interface position at temperature u_{ip}.

The Figure 3.7 compares the results of numerical solution of Stefan problem (a), solution of loose(b) and tight coupling(c). We further discuss the results in chapter 4.
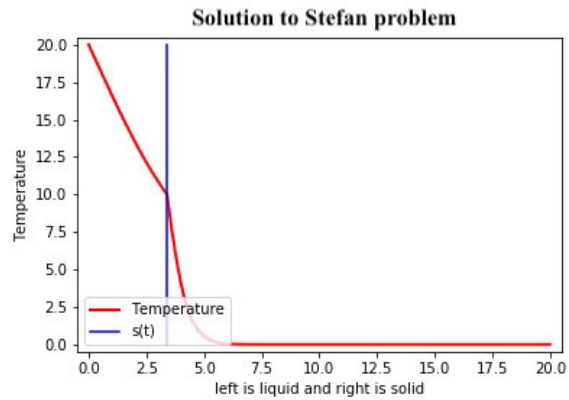
(a)
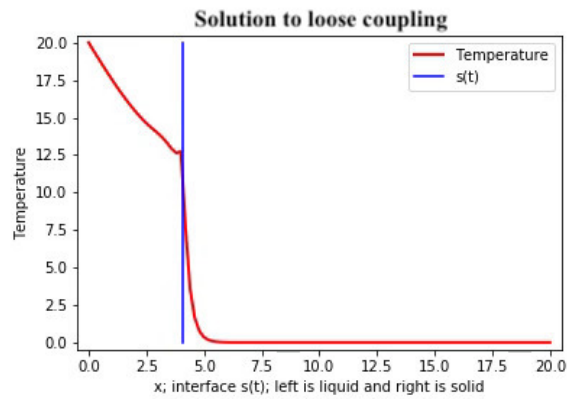
(b)
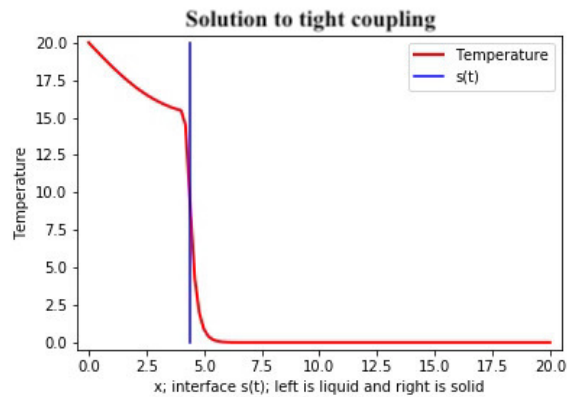
(c)

Figure 3.7: Comparing the results of (a) Numerical solution of two phase Stefan problem, (b) Solution of loose coupling, (c) Solution of tight coupling at t ≈ 1. The red line represents temperature and the blue line represents the position of the interface.

Chapter 4

Discussion

4.1   Numerical tests

Figure 3.7 in chapter 3 shows the results of numerical solution of Stefan problem (a), solution of loose (b) and tight coupling (c). We observe that we cannot draw conclusions from the results of coupling solutions (b) and (c) as both the temperature and position of the interface in coupling methods does not look similar to the reference (a). Therefore, we further analyse the results in the following sections. The convergence rate is given by the ratio between the discontinuous diffusion coefficients (k_l/k_s) [10]. The convergence properties of the coupling problem have been extensively studied in the case of constant and continuous diffusion coefficients [12]. There is another parameter from the coupling equation (3.15), latent heat content H_f which explains about the energy transfer between the liquid and solid subdomains. Moreover, H_f effects the speed of the movement of the interface, shown in Figures. Therefore, we study the behaviour of the coupling methods and Stefan problem with respect to the parameters of the diffusion equation. In this chapter, we conduct sensitivity experiments for the parameters involved and so we considered different ratios of diffusion coefficients $k_l/k_s \approx 1$, $k_l/k_s = 2,5,10$ and different values of latent heat $H_f = 1,10$ and 20 and compared the results of numerical solution of Stefan problem and coupling solutions. Also, we analysed the results of interface position, L^∞ norm for interface and L^2 norm for temperature in section 4.1.1, 4.1.2 and 4.1.3 respectively.

4.1.1 Interface Position

Figure 4.1 shows the results for the interface position comparing the loose (blue) and tight (red) coupling methods to the solution of Stefan problem as the reference solution (black) for different ratios of diffusion coefficients (k_l/k_s) and with different values of H_f. In Figure 4.1, we observe that when the ratio of (k_l/k_s) $\approx$ 1 in (a), (b), (c), the interface position s(t) for tight moves closer to the reference as the H_f value increases, whereas s(t) for loose moves away from the reference as the H_f value increases. Also, when the ratio of diffusion coefficients $k_l/k_s = 2$ in (d), (e), (f), the position of interface s(t) for tight moves closer and moves away for loose when compared to the reference as the latent heat H_f increases. However, when the ratio $k_l/k_s = 5$ in (g), (h), (i), we observe that the s(t) for tight moves away from the reference as H_f increases, whereas s(t) for loose moves close to the reference as H_f increases. Similarly, for $k_l/k_s = 10$ in (j), (k), (l), the interface position for tight gradually deviates away from the reference, whereas it moves closer for loose as the H_f value increases.

Therefore, from the above results, we can say that as the ratio of diffusion coefficients of liquid and solid domains k_l/k_s increases, the solution for loose coupling looks better as the latent heat H_f increases. Whereas, the solution of tight coupling looks better for the smaller ratios of diffusion coefficients ($k_l/k_s \approx 1$, k_l/k_s) = 2) as the latent heat increases. Though the literature [10] shows that the convergence rate to the reference increases using Schwarz iteration method when the ratio of the discontinuous diffusion coefficients (k_l/k_s) $\approx$ 1. However this is true for a fixed and non overlapping interface. In our case, we have compared different coupling methods with moving boundary interface, thereby the results shows the tight coupling looks better for smaller ratios of diffusion coefficients and loose coupling solution looks better for relatively larger ratios, when compared to the reference. Also, as H_f increases, the amount of energy transfer between the subdomains increases, which

could have increased the movement of the interface $s(t)$ towards the reference for tight when $k_l/k_s \approx 1$ and for loose when k_l/k_s increases to 5,10.
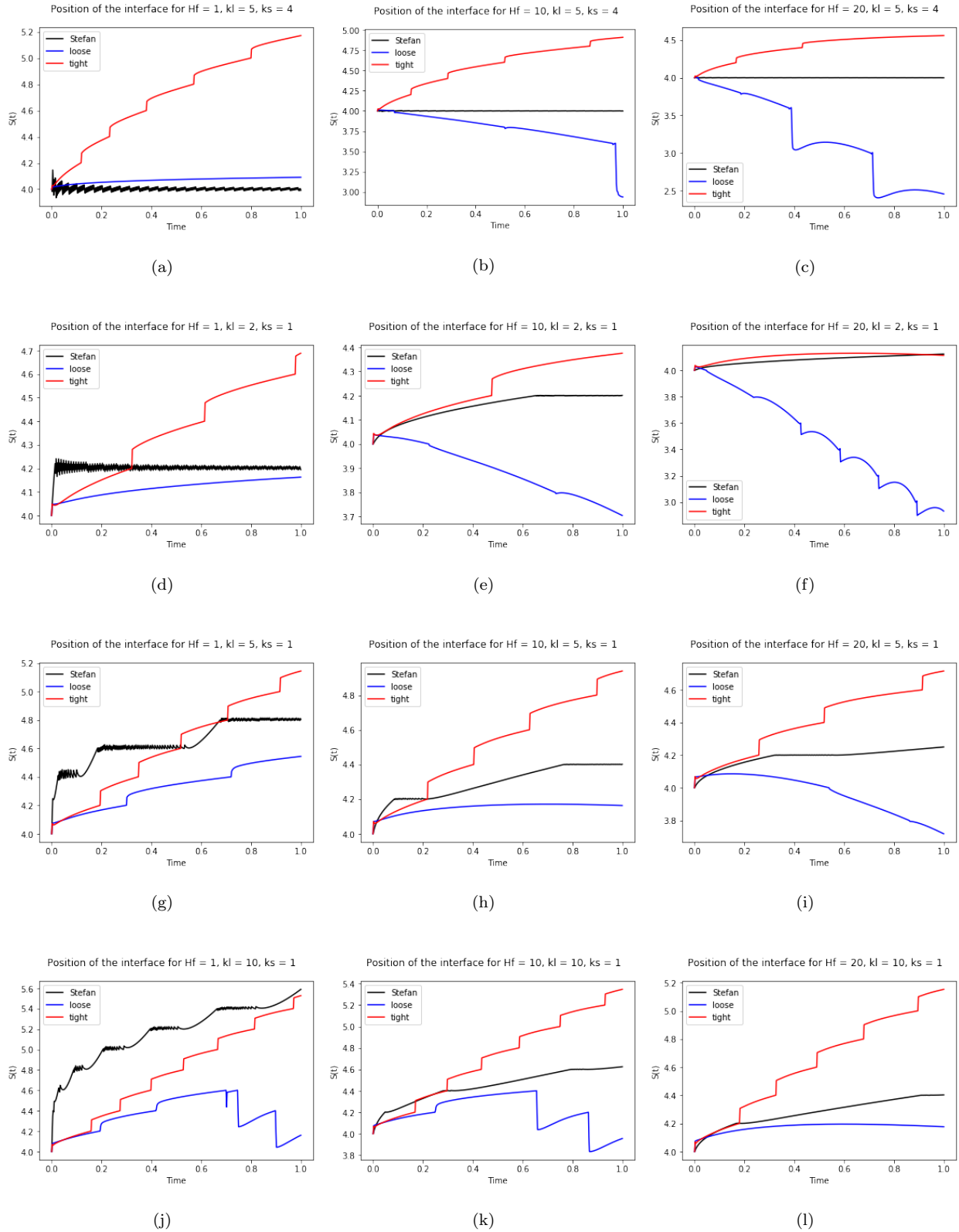
Figure 4.1: Comparing interface position of Stefan problem (black),loose coupling (blue) and tight coupling solutions (red) at different ratios of diffusion coefficients and latent heat of fusion Hf. $k_l/k_s \approx 1$ for (a) Hf = 1, (b) Hf = 10, (c) Hf = 20. k_l/k_s = 2 for (d) Hf = 1, (e) Hf = 10, (f) Hf = 20. k_l/k_s = 5 for (g) Hf = 1, (h) Hf = 10, (i) Hf = 20. k_l/k_s = 10 for (j) Hf = 1, (k) Hf = 10, (l) Hf = 20.

4.1.2 L^∞ - norm

In this section, we consider L^∞ norm for the interface in order to detect the phase errors more clearly. Let $s(t)_{\text{reference}}$ be the interface position $s(t)$ for the Stefan problem and $s(t)_{\text{coupling}}$ be the interface position of loose (blue) and tight (red) coupling methods. The L^∞ norm for the interface $s(t)$ at time t^n is given by

$$||s(t)||_{L^\infty} = \max[s(t^n)_{\text{reference}} - s(t^n)_{\text{coupling}}] \tag{4.1}$$

Figure 4.2 shows the results of L^∞ norm for the interface comparing between the reference to loose (in blue) and tight (red) coupling solutions for different ratios of diffusion coefficients $(k_l/k_s) = $ (a) ≈ 1, (b) 2, (c) 5, (d) 10 and different values of latent heat $H_f = 1$, 10 and 20. In Figure 4.2 in (a), (b), and (c), when the ratio $k_l/k_s \approx 1$ and as the H_f increases, we observe that the error for loose slightly increases, whereas for tight, the error approximately maintained at zero as H_f increases. Also, when the ratio $k_l/k_s = 2$ in (d), (e), and (f), the error for tight reaches to zero and the error for loose gradually increases as the H_f value increases. However, when $k_l/k_s = 5$ in (g), (h), (i), as H_f increases, it shows that the error for both tight and loose slightly deviates from zero but when compared to (a), (b) and (c), it seems that loose is better in (g), (h), (i). Similarly, in (j), (k) and (l), when the ratio $k_l/k_s = 10$, we observe that the error for loose reaches to approximately zero as H_f increases, whereas for tight, the error slightly deviates from zero.

From the results, we can say that when the ratio $k_l/k_s \approx 1$ and $k_l/k_s = 2$, tight coupling looks better with zero error as H_f increases. Whereas, as the ratio increases $(k_l/k_s = 5, 10)$, we observe that the error for loose reaches to zero as H_f increases. From the above results, we may say that, as the value of H_f increases, the L^∞ error norm reaches approximately to zero for tight when the ratio $k_l/k_s \approx 1$ and $k_l/k_s = 2$. But as the ratio k_l/k_s increases, the L^∞ error norm reaches approximately to zero for loose as the value of H_f increases. As explained in section 4.1.1, as the latent heat H_f increases, the amount of energy transfer

between the subdomains increases, which could have increased the movement of the interface $s(t)$ towards the reference for tight when $k_l/k_s \approx 1$ and for loose when k_l/k_s increases to 5, 10. Therefore, resulting in approximately zero L^∞ norm for tight when the ratio $k_l/k_s \approx 1$ and $k_l/k_s = 2$. Similarly, the increased value of latent heat H_f resulted to approximately zero L^∞ norm for loose when k_l/k_s increases to 5, 10.

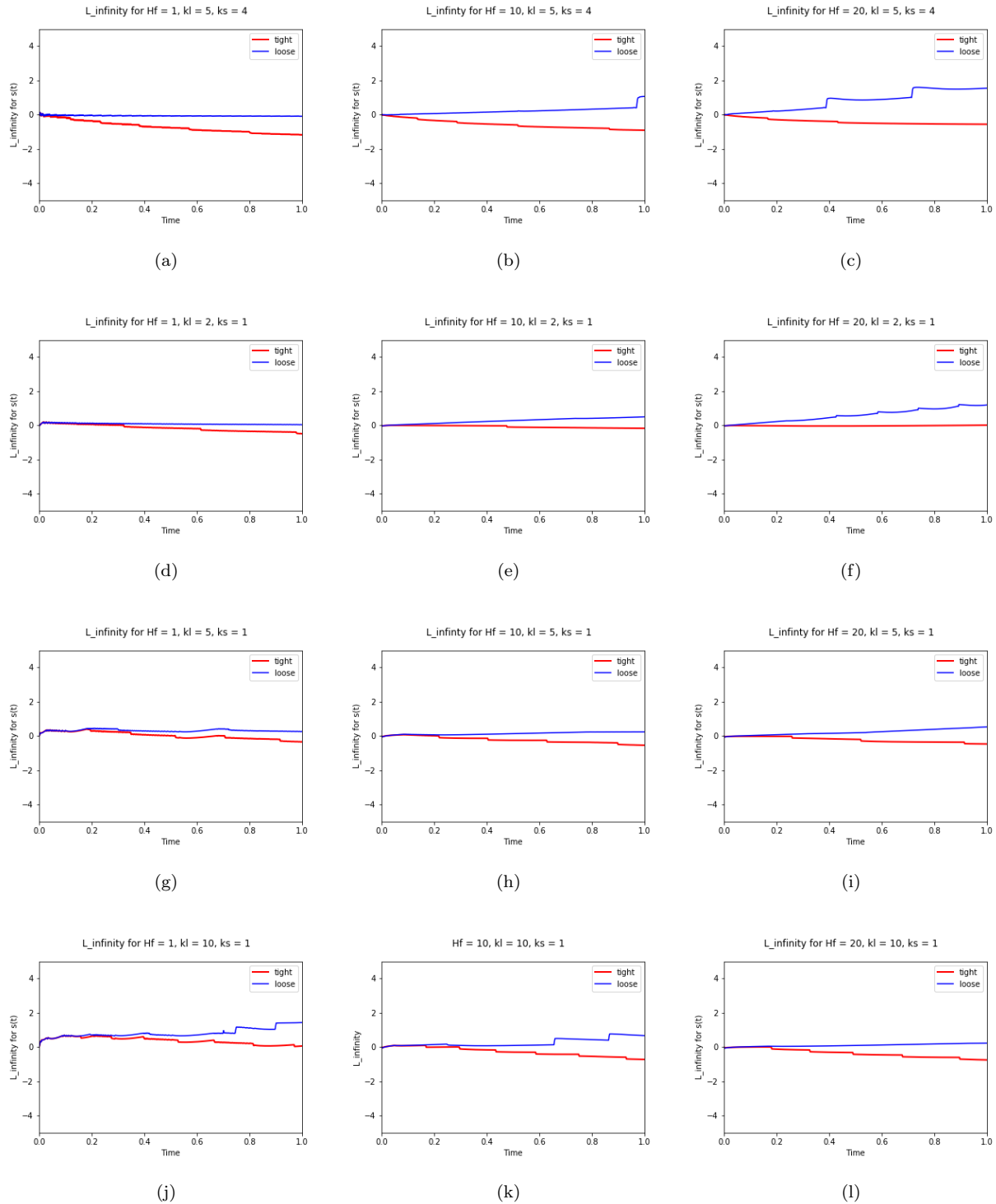Figure 4.2: Comparing L_infinity of Stefan problem (Black),loose coupling (Blue) and tight coupling solutions (Red) at different ratios of diffusion coefficients and latent heat of fusion Hf. $k_l/k_s \approx 1$ for (a) Hf = 1, (b) Hf = 10, (c) Hf = 20. $k_l/k_s = 2$ for (d) Hf = 1, (e) Hf = 10, (f) Hf = 20. $k_l/k_s = 5$ for (g) Hf = 1, (h) Hf = 10, (i) Hf = 20. $k_l/k_s = 10$ for (j) Hf = 1, (k) Hf = 10, (l) Hf = 20.

4.1.3 L^2-error norm

In order to investigate the relative error between the reference and the coupling methods, we consider L^2-error norm, i.e., the root mean square error, for the temperature. Let $u_{reference}$ be the numerical solution of the Stefan problem and $u_{coupling}$ be the solution for loose and tight coupling methods. The relative L^2-error norm at time t^n for nx (number of grid points) is given by

$$||u_{reference} - u_{coupling}||_{L^2}^2 = \frac{\sum_{i=1}^{nx} |u_{i,reference} - u_{i,coupling}|^2}{\sum_{i=1}^{nx} |u_{i,reference}|^2} \qquad (4.2)$$

Figure 4.3 compares the relative error (L^2 norm) between the coupling methods (loose (blue) and tight (red) and reference solution for different ratios of diffusion coefficients((k_l/k_s) and values of latent heat H_f. In Figure 4.3 (a), (b) and (c), we observe that, as H_f increases for the ratio $k_l/k_s \approx 1$, the relative error for tight gradually decreases, but increases for loose. The jump in (c) for loose is due to large time step. Also, when the ratio $k_l/k_s = 2$ in (d), (e), (f), the relative error for tight gradually decreases and the error for loose increases. However, when the ratio of diffusion coefficients $k_l/k_s = 5$, in (g), (h), (i), we observe that as the value of H_f increases, the relative error for tight increases and decreases for loose. Similarly, when $k_l/k_s = 10$ in (j), (k) and (l), the relative error increases for tight and decreases for loose as the value of H_f increases.

From these results, we can say that, as the value of H_f increases, the relative error decreases for tight when the ratio $k_l/k_s \approx 1$ and $k_l/k_s = 2$. Whereas, the relative error decreases for loose when the ratio $k_l/k_s = 5, 10$ and value of H_f increases. As explained in section 4.1.1 and 4.1.2, as H_f increases, the amount of energy transfer between the subdomains increases, which could have increased the movement of the interface s(t) towards the reference for tight when $k_l/k_s \approx 1$ and $k_l/k_s = 2$. Similarly, increases the movement of interface towards the reference for loose when k_l/k_s increases to 5 and 10. This movement of the interface position could have effected the value of temperature at the interface from

equations 3.16 and 3.17 for loose and tight coupling respectively. Thereby, producing similar results as in 4.1.1 and 4.1.2 i.e; resulted in less relative error for tight when the ratio $k_l/k_s \approx 1$ and $k_l/k_s = 2$ as H_f increases and less relative error for loose when ratio increases to 5 and 10 when the latent heat H_f increases.

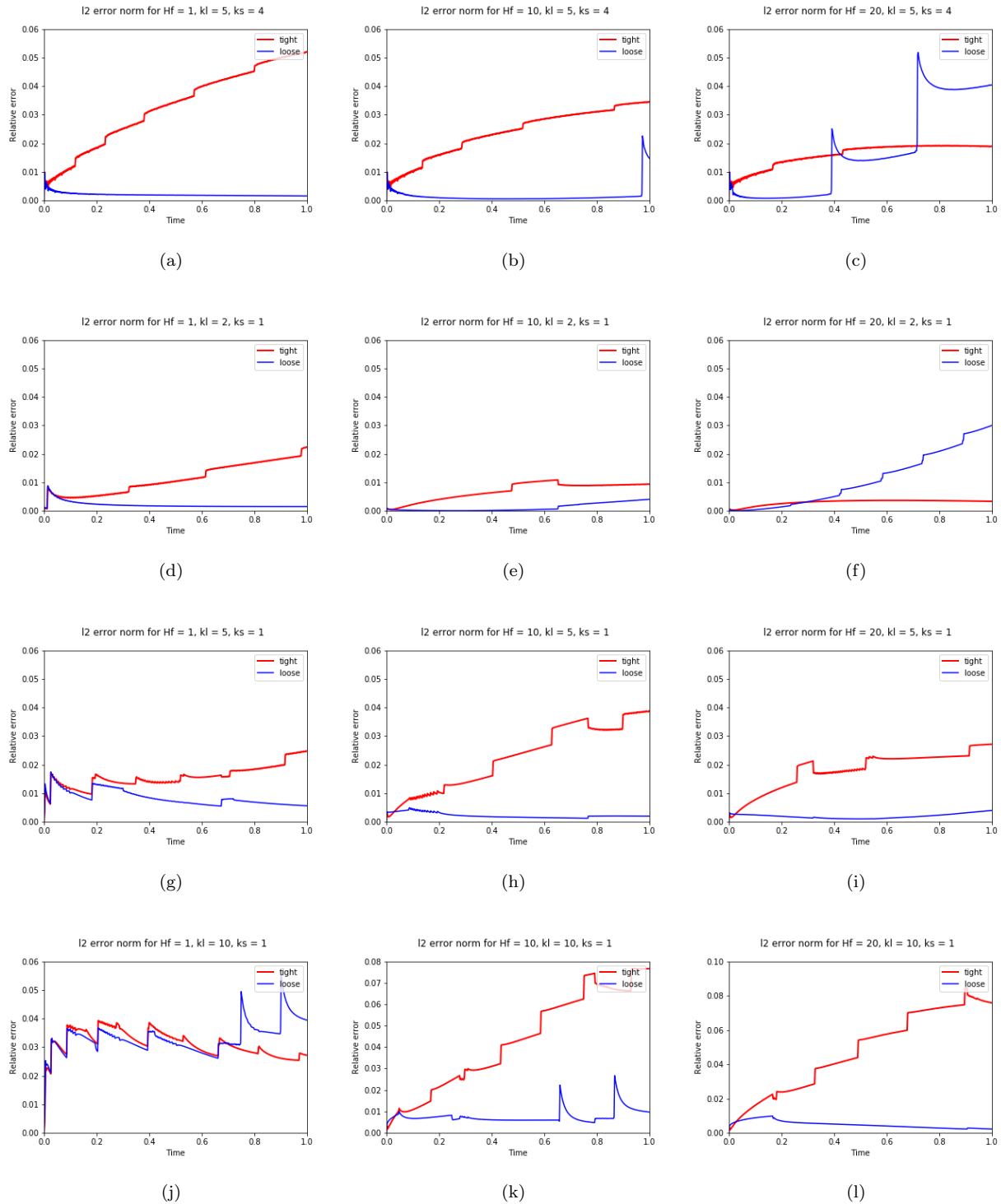Figure 4.3: Comparing L^2 error between the reference and loose (blue) and tight coupling (red) solutions at different ratios of diffusion coefficients and latent heat of fusion Hf. $k_l/k_s \approx 1$ for (a) Hf = 1, (b) Hf = 10, (c) Hf = 20. $k_l/k_s = 2$ for (d) Hf = 1, (e) Hf = 10, (f) Hf = 20. $k_l/k_s = 5$ for (g) Hf = 1, (h) Hf = 10, (i) Hf = 20. $k_l/k_s = 10$ for (j) Hf = 1, (k) Hf = 10, (l) Hf = 20.

4.2   Conclusions

One of the conclusions of our thesis: The studies from [33], [34], [63],[35] showed that a large overlap between the sub-domains can improve the accuracy of a coupling method with fixed interface. However, our results showed that an increase of overlap in tight coupling with a moving interface may not contribute to the improvement of coupling solution. It can be explained as follows: The results of sensitivity experiments looks better for tight coupling with the smaller ratios of diffusion coefficients ($k_l/k_s \approx 1$ and $k_l/k_s = 2$) and as the latent heat value (H_f) increases from 1 to 20. With smaller diffusion ratios, we observed that the tight coupling solutions shows kink at the interface, which allows for a sharp transition. Also, as the latent heat H_f increases, the amount of energy transfer between the sub-domains increases, which could have increased the movement of the interface s(t) towards the reference for tight coupling. Moreover, due to the large overlap and interpolation at the interface, the kink gets smoothed between the subdomains, resulting in smaller deviation from the reference compared to loose coupling. However, these results are not accurate as the smoothing of kink due to large overlap and interpolation does not represent the physical behaviour. As the ratio increases ($k_l/k_s = 5$ and $k_l/k_s = 10$), the kink between the two subdomains gets more pronounced at the interface. Also, as the H_f increases, even with larger overlap and interpolation at the interface, the tight coupling solution does not improve its solution when compared to results with smaller ratios. For higher ratios, the loose coupling solution with one grid point overlap looks better compared to tight coupling, producing less deviation from interface and less error as the latent heat increases. From these results, we conclude that the increase in overlap with a moving interface (tight coupling) may not improve the coupling solution due to the pronounced kinks formed due to higher ratios of diffusion coefficients and the moving boundary at the interface.

Other part of the conclusion of our study: The studies from [10], [11], [9] showed that

the iterative method provides stable and consistent coupling solution with a fixed interface between the subdomains. Our study attempts to see if we could improve the coupling using iterative method. We used iteration method to update the boundary conditions at the moving interface. However, from the results we noticed that the pronounced kink formed due to the diffusion coefficients and moving interface does not contribute to the improvement of solution, even though the iterations were used at the interface. Therefore, we conclude that the iterative method may not improve the coupling solution with a moving interface, at least with our simple test case.

Appendix A

Domain decomposition method (DDM)

A.1   Introduction

In Appendix A and B, we describe our preliminary results which explains our failed ideas to test coupling. In Appendix A, we started with implementing DDM to a stationary problem, 1D Poisson equation[66] and later extended DDM to time dependent problem, 1D parabolic equation[10], [67]. These results are for a fixed interface, comparing with larger overlap and with a number of iterations. Later, we tried to couple shallow water equation for atmosphere and ocean, which did not work because there is only one point (in the vertical) that can be coupled - so no freedom to iterate over. Therefore, we used coupling idea based on [68] and [69], further explained in A.2.3. As mentioned in Chapter 1, our study is intended to see if iterative method could improve the coupling solution for a problem with a moving interface. In order to implement this, we used a interface condition (B.1) from the literature [58]. The interface condition (B.1) is valid only for the case of fixed interface and therefore we implemented a criteria to move the interface. However, it is not accurate way to represent the moving interface, but nevertheless important to document our failed idea (Appendix B).

In 1870, H.A.Schwarz introduced an iteration over a decomposition of the domain, for solving Laplace's equation [13]. In the earlier, the use of this idea was to prove the existence and uniqueness of the solution on domains that are unions of simple geometries [63], [70]. More than a century later, domain decomposition methods came back to interest and are now an

active area of research, for developing efficient solvers for partial differential equations. The idea of Schwarz decomposition methods is to separate the original problem on a domain into sub-domains (sub-problems) which can be solved separately. An iterative process is then applied to achieve convergence to the solution of the original problem. There are two main classical Schwarz methods at the continuous level: the alternating Schwarz method invented by Schwarz in [71] as a mathematical tool, and the parallel Schwarz method introduced by [36] for the purpose of parallel computing. The convergence rate of these Schwarz methods depends on the transmission conditions employed between subdomains [13]. Domain decomposition methods are divided into overlapping and non overlapping methods. These methods uses alternatively the solution on one subdomain to update the Dirichlet data of the other. The rate of convergence of Schwarz method depends upon the overlapping length between the subdomains [62]. Originally these methods are introduced for stationary problems, but recently extended to time dependent problems to provide a global-in-time Schwarz method [13]. According to Lemarie [9], the adaptation of Schwarz domain decomposition methods obtain a stable and consistent coupling method. These methods are now widely used for coupling problems.

In this Chapter, we explain the implementation of the domain decomposition methods to 1D poisson, parabolic and shallow water equations. The preliminary results compares the solution of these equations between with and without decomposition methods, however there is no reference to compare these solutions. Also, our interest lies in understanding the coupling using iterative method for a moving interface (refer to motivation in Chapter 1). Therefore, after a rigorous literature review, we found a Stefan problem, with a moving interface. It provides a consistent and energy conserving solution (explained in Chapter 2). As a result, we use the solution of Stefan problem as a reference to our coupling methods (explained in Chapters 3 and 4).

Figure A.1 shows the original domain used by Schwarz, with the associated domain decomposition into two subdomains, which are geometrically much simpler, namely a disk Ω_1 and
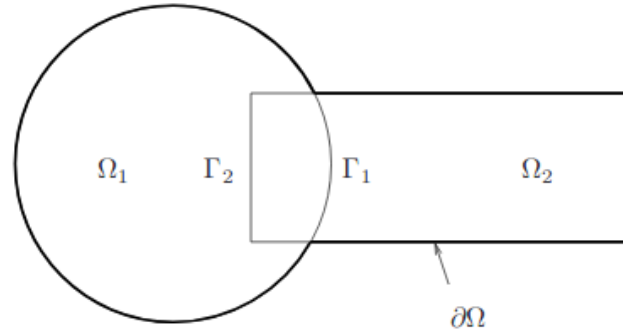
Figure A.1: The Figure is taken from [13]. The first domain decomposition method was introduced by Schwarz for a complicated domain,composed of two simple ones, namely a disk and a rectangle.

a rectangle Ω_2, with interfaces $\Gamma_1 = \partial\Omega_1 \cap \Omega_2$ and $\Gamma_2 = \partial\Omega_2 \cap \Omega_1$. The equations below are taken from [13].

$$\Delta u = 0 \quad \text{in} \quad \Omega, \quad u = g \quad \text{on} \quad \partial\Omega \tag{A.1}$$

where $\Delta u = 0$ is the Laplace equation on a bounded domain Ω with Dirichlet boundary conditions $u = g$ on $\partial\Omega$. By using alternating Schwarz method, an iterative method which only uses solutions on the disk and the rectangle, where solutions can be obtained using Fourier series [13].

$$\Delta u_1^{n+1} = 0 \quad \text{in} \quad \Omega_1, \tag{A.2}$$

$$\Delta u_2^{n+1} = 0 \quad \text{in} \quad \Omega_2, \tag{A.3}$$

$$u_1^{n+1} = u_2^n \quad \text{on} \quad \Gamma_1, \tag{A.4}$$

$$u_2^{n+1} = u_1^{n+1} \quad \text{on} \quad \Gamma_2, \tag{A.5}$$

The method starts with an initial guess u_2^0 along Γ_1 (Figure A.1), and then computes iteratively for n = 0,1,..the iterates u_1^{n+1} and u_2^{n+1} according to the algorithm (A.2 - A.5), where it is omitted from now on for simplicity that both u_1^{n+1} and u_2^{n+1} satisfy the given Dirichlet condition in (A.1) on the outer boundaries of the respective subdomains. There is another method, called parallel Schwarz method, in contrast to the alternating Schwarz

method. From the Figure A.1, the method is given by [13]

$$\Delta u_1^{n+1} = 0 \quad \text{in} \quad \Omega_1, \tag{A.6}$$

$$\Delta u_2^{n+1} = 0 \quad \text{in} \quad \Omega_2, \tag{A.7}$$

$$u_1^{n+1} = u_2^n \quad \text{on} \quad \Gamma_1, \tag{A.8}$$

$$u_2^{n+1} = u_1^n \quad \text{on} \quad \Gamma_2, \tag{A.9}$$

The only change is the iteration index in the second transmission condition, which makes this method parallel: given initial guesses u_1^0 and $u_2{}^0$, one can now simultaneously compute, for n = 0,1,.. both subdomain solutions in parallel. In this simple two subdomain case, there is, however, no gain, since the sequence computed on Ω_1 every two steps coincides with the sequence computed on Ω_1 by the alternating Schwarz method.

A.2 Application of DDM

A.2.1 Poisson equation

In this section, we discuss the idea of domain decomposition method to 1D Poisson's equation [66]. Consider the problem associated with finding the solution of poisson's equation for a rectangle. The problem is solved according to [66]:

$$\Delta u = f \quad \text{in} \quad \Omega \tag{A.10}$$

$$u = g \quad \text{on} \quad \partial\Omega$$

The basic strategy of the domain decomposition procedure is to decompose the region into two pieces Ω_1 and Ω_2 and construct a solution to (A.10) by taking the union of solutions to (A.10) on sub-domains. If the domain is split up into two pieces, then the sub-domain problems are specified as follows:

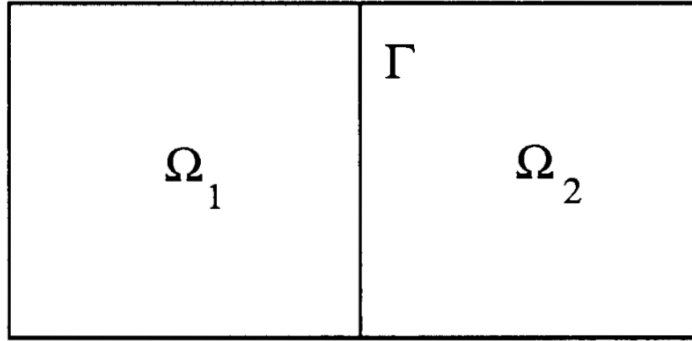$$\Delta u_i = f_i \quad \text{in} \quad \Omega_i \tag{A.11}$$

.

Figure A.2: The Figure is taken from[66]. Basic strategy of Domain decomposition method

$$u_i = g \quad \text{on} \quad \partial\Omega_i/\Gamma$$

$$u_i = u_\Gamma \quad \text{on} \quad \partial\Gamma$$

for i = 1,2 and Γ is the interface between the two sub-domains (Figure A.2).The difficulty in implementing this technique is the determination of the boundary values u_Γ. So, they[66] find the equations which satisfy the u_Γ and then solve these equations. With the u_Γ determined, the complete solution over the domain is obtained by solving (A.11) for u_1 and u_2. The equations which determine u_Γ are the equations which ensure that if they are solved, and these values are used in the two boundary value problems (A.11), then the resulting solutions combine to form a solution on the whole domain. For the two solutions of (A.11), u_1 and u_2 are to be combined to form a solution of the problem on the whole domain and they must be continuous and their normal derivatives must also be continuous across the interface Γ. The condition at the overlap region Γ are taken from [66] :

$$u_1 = u_2 \quad \text{on} \quad \Gamma \tag{A.12}$$

$$\frac{\partial u_1}{\partial n} = -\frac{\partial u_2}{\partial n} \quad \text{on} \quad \Gamma \tag{A.13}$$

We assume that $u_1 = u_2 = u_\Gamma$ along Γ, so that (A.12) is satisfied. These conditions are called the "transmission" or "flux" boundary conditions, which determine the equations for u_Γ.

Now in Figure A.3, we considered 100 grid points for the 1D domain, the whole domain x $\in$ (a,b) is divided into two sub-domains. We discretize the equation (A.14) using implicit method using boundary conditions (A.15). Here we observe from the equations that we use same coefficients unlike in the Stefan problem , loose and tight coupling methods we have described in Chapter 2 - 4. Below are the 1D Poisson equation A.14 and boundary conditions A.15 we considered.

$$-\frac{\partial^2 u_i}{\partial x^2} = f, \quad i = 1, 2 \quad x \in (a, b) \tag{A.14}$$

$$u_1(a) = 0, \quad u_2(b) = 1 \tag{A.15}$$

We write the linear system of equations in matrix-vector form Au = f, where A is coefficient matrix, u is the solution matrix and f is vector matrix.

$$\begin{pmatrix} -1 & -2 & -1 & 0 & . & . \\ 0 & -1 & -2 & -1 & 0 & \\ 0 & 0 & -1 & -2 & -1 & \\ ... & ... & ... & ... & ... & \\ ... & ... & ... & ... & ... & \\ 0 & 0 & . & -1 & -2 & \end{pmatrix} \begin{pmatrix} u_0 \\ ... \\ ... \\ ... \\ ... \\ u_n \end{pmatrix} = \begin{pmatrix} f_0 \\ ... \\ ... \\ ... \\ ... \\ f_n \end{pmatrix} \tag{A.16}$$

The matrix is similar for the two subdmomains which computes the solution for Poisson equation. Now, at the overlap region we consider Dirchlet boundary conditions (A.17) and (A.18) to exchange values at the interface at each iteration between the sub-domains. The Boundary conditions at the interface are specified as follows:

$$u_1^{(n+1)} = u_2^{(n)} \tag{A.17}$$

$$u_2^{(n+1)} = u_1^{(n+1)} \tag{A.18}$$

Figure A.3 compares with and without domain decomposition methods for the solution of 1D Poisson equation. We considered 10 iterations for the decomposition methods, and compared

to the solutions by increasing the overlap region. However there is no reference solution to compare both these results.

A.2.2 Parabolic equation

In the similar way as above sub section A.2.1, we consider DDM for 1D parabolic equation. We divide the whole domain $u[0, \pi]$ into two subdoamins u_1 and u_2 with the space step Δx and the time step Δt, to solve the following 1D parabolic equation (A.19). We discretize the equation using finite differences and with the following initial condition (A.20) and boundary conditions (A.21).

$$\frac{\partial u_i}{\partial t} = K \frac{\partial^2 u_i}{\partial x_i^2}, \quad i = 1, 2 \quad x \in (0, \pi) \quad , \quad t \in (0, T) \tag{A.19}$$

$$u_1(x, 0) = u_2(x, 0) = \sin(x), \quad x \in (0, \pi) \tag{A.20}$$

$$u_1(0, t) = u_2(\pi, t) = 0, \quad t \in (0, T] \tag{A.21}$$

We write the linear system of equations in matrix-vector form $Au = f$ similar to (A.16), where A is coefficient matrix, u is the solution matrix and f is vector matrix. The matrix is similar for the two sub-domains ($Au_1^{n+1} = u_1^n$ and $Au_2^{n+1} = u_2^n$) which computes the solution for Parabolic equation.

$$\begin{pmatrix} 1+2p & -p & 0 & . & . \\ -p & 1+2p & -p & 0 & . \\ 0 & -p & 1+2p & -p & . \\ ... & ... & ... & ... & ... \\ ... & ... & ... & ... & ... \\ 0 & 0 & . & -p & 1+2p \end{pmatrix} \begin{pmatrix} u_0^1 \\ ... \\ ... \\ ... \\ ... \\ u_n^{t+1} \end{pmatrix} = \begin{pmatrix} u_0^0 \\ ... \\ ... \\ ... \\ ... \\ u_n^t \end{pmatrix} \tag{A.22}$$

where $p = k \frac{\Delta t}{(\Delta x)^2}$ Now, at the overlap region we consider Dirchlet boundary conditions (A.23) to each exchange values at the interface at each iteration between the subdomains.
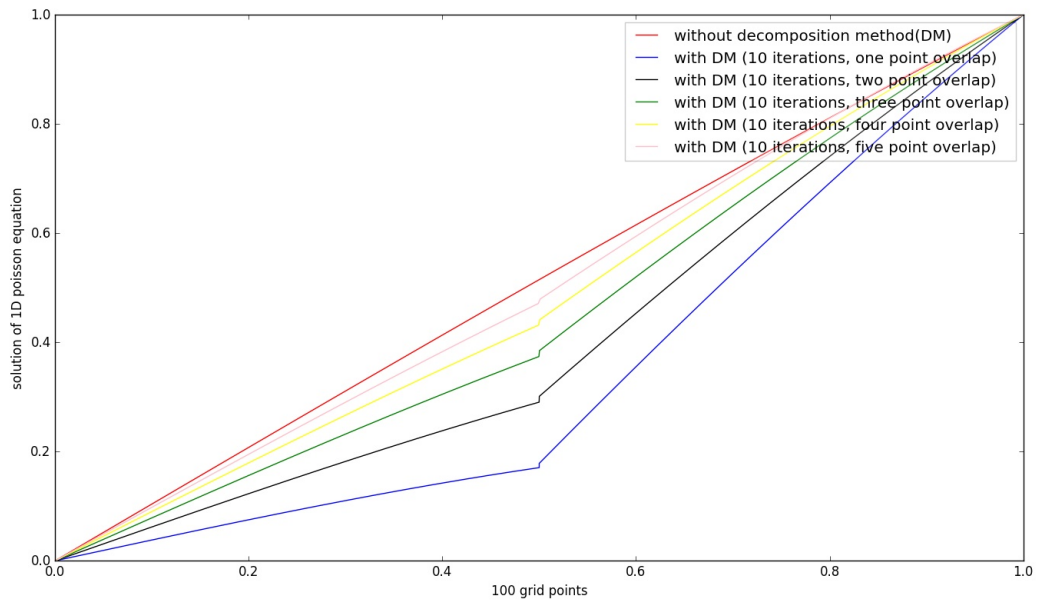
Figure A.3: Comparing solution of Poisson equation with and without domain decomposition method. x axis denotes grid points and y axis denotes the solution of Poisson equation.

The Boundary conditions at the interface are specified as follows:

$$u_1^{n+1} = u_2^n, \quad u_2^{n+1} = u_1^{n+1} \tag{A.23}$$

Figure A.4 represents the preliminary result showing the implementation of domain decomposition to the solution of 1D heat equation at each time step where $t_{20} > t_{19} > ...t_1$. However there is no reference (like Stefan problem) to compare these solutions.

A.2.3   Shallow water equation

Shallow water equations are hyperbolic type of equations. The equations are derived from depth-integrating the Navier Stokes equations, in the case where the horizontal length scale is much greater than the vertical length scale. The shallow water equations are derived from equations of conservation of mass and conservation of linear momentum (the NavierâStokes equations). Situations in fluid dynamics where the horizontal length scale is much greater than the vertical length scale are common, so the shallow water equations are widely applicable. They are used with Coriolis forces in atmospheric and oceanic modelling, as a simplification of the primitive equations of atmospheric flow.

We tried to couple shallow water equation for atmosphere and ocean, which did not work because there is only one point (in the vertical) that can be coupled - so no freedom to iterate over. Therefore, we used coupling idea based on [68] and [69]. In this section, we consider two superposed one-layer fine-resolution shallow-water models and their coupling according to [68] and [69]. The upper layer represents the atmosphere and the lower layer the ocean, with their only interaction being through a frictional force at the interface, which is parametrized by a quadratic drag law. In this paper [69], the drag coefficient over the surface according is based on [72]. This physical model can be described by two coupled
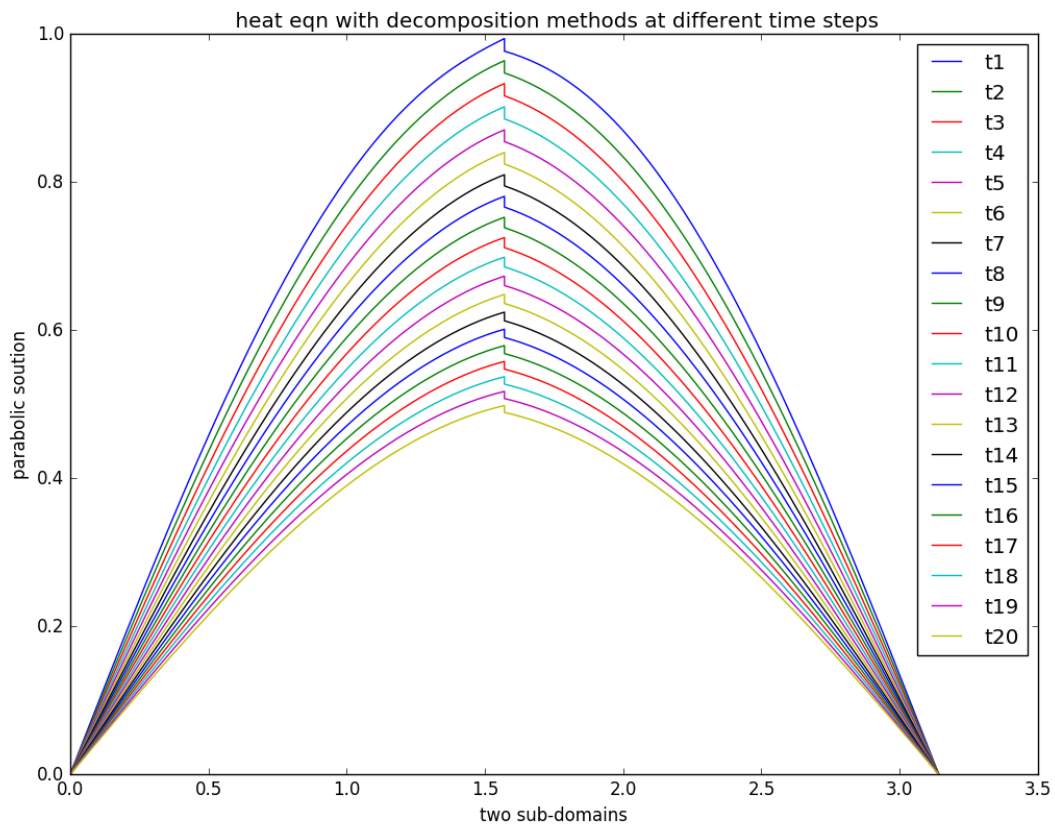
Figure A.4: Solution of 1D Parabolic equation with domain decomposition method at $t_{20} > t_{19} > ..t_1$. x axis denotes grid points and y axis denotes the solution of Parabolic equation.

reduced-gravity shallow water equations[69],

$$\frac{\partial u^k}{\partial t} = g^k \frac{\partial h^k}{\partial x} + F_x^k \tag{A.24}$$

$$\frac{\partial h^k}{\partial t} = H^k \frac{\partial u^k}{\partial x} \tag{A.25}$$

where

k represents atmosphere and ocean respectively(a,o)

u is the velocity in the x direction, or zonal velocity

h is the height deviation of the horizontal pressure surface from its mean height H: $\eta = $ H

+h

H is the mean height of the horizontal pressure surface

g is the acceleration due to gravity

Initially the atmosphere is considered to be moving with a constant velocity 1m/s and ocean

is at rest. The equations are discretized by Lax-Friedrichs schemes with initial conditions

for velocity (A.26) and height (A.27) for atmosphere and ocean. The boundary conditions

are considered to be periodic [69].

$$u^a(x, 0) = 1, \quad u^o(x, 0) = 0 \tag{A.26}$$

$$h^a(x, 0) = \exp(-(x-50)^2), \quad h^o(x, 0) = 0 \tag{A.27}$$

Concerning the atmosphere, a Dirichlet boundary condition is imposed, which means the
wind is supposed to vanish at the surface, without considering the direct effect of ocean
currents. For the ocean, a Neumann boundary condition is imposed; that is, the shear of the
atmosphere on the ocean is applied to the ocean. In one-way interactions, the shear applied
to the atmosphere neglects the effects of ocean currents; the ocean is a rough motionless
surface. In two-way interactions, the shear applied to the atmosphere is opposite the shear
applied to the ocean. Here [69], one way interaction is considered where the two layers are
only coupled by frictional forces at the interface, parameterized by a quadratic drag law.

The frictional acceleration between the two layers are taken from [69] and are defined as

$$F_x^k = \pm \frac{1}{\rho^k h^k}(f_x^k) \tag{A.28}$$

where f_x is the surface force depending on x, ρ^a and ρ^o are densities for atmosphere and ocean respectively. The shear applied to the ocean is calculated using the velocity difference between wind and ocean current

$$f_x^o = \rho^a C_d |u|(u^o - u^a) \tag{A.29}$$

where $|u| = \sqrt{(u^o - u^a)^2}$. The drag coefficient is constant in our calculations : $C_d = 8 \times 10^{-4}$ is a classical value [72]. We have considered one-way interaction, shear applied to the atmosphere neglects the effects of ocean currents

$$f_x^a = \rho^a C_d \sqrt{(u^a)^2}(-u^a) \tag{A.30}$$

Figure A.2.3 represents the initial conditions for velocity and height profile for atmosphere and ocean. From Figure A.6, we observe that at time t = 1, the coupling between lower atmosphere and upper ocean surfaces through frictional forces.

For more realistic representation, we drop the assumption which states that atmospheric pressure is constant. For a shallow homogeneous ocean, the momentum equation becomes

$$\frac{\partial u^o}{\partial t} = g^o \frac{\partial h^o}{\partial x} + g^a \frac{\partial h^a}{\partial x} \tag{A.31}$$

$$\frac{\partial h^o}{\partial t} = H^o \frac{\partial u^o}{\partial x} \tag{A.32}$$

These are similar to earthquake generated tsunamis, but caused by air pressure disturbances often caused by fast moving weather. Meteotsunamis are generated by meteorological events, particularly moving pressure disturbances due to squalls, thunderstorms, frontal passages and atmospheric gravity waves. Relatively small initial sea-level perturbations, of the order of a few centimetres, can increase significantly through multi-resonant phenomena to create destructive events through the superposition of different factors. These disturbances can

generate waves in the ocean that travel at the same speed as the overhead weather system. A key factor in the generation of meteotsunamis is the speed of the pressure disturbance relative to the phase speed of long waves in the ocean. When the speed of the pressure disturbance approaches the long-wave speed, the coupled wave becomes amplified: an effect termed Proudman resonance [73]. In Figure A.7, we represent the effects of atmosphere pressure on the ocean velocity and height profile.

These coupling ideas are the preliminary results based on research performed on a fixed interface [66], [10]. Also, the iteration method applied to 1D poisson and parabolic equation are with same coefficients for both the subdomains. As mentioned above, we could not apply the iterative method to shallow water equations and we used the coupling based on [68] and [69]. Our interest lies in coupling two subdomains with different diffusion coefficients with a moving interface in order to model a more "realistic" test case. Now, in Appendix B, we further explain our failed ideas for coupling two subdomains with a moving interface.
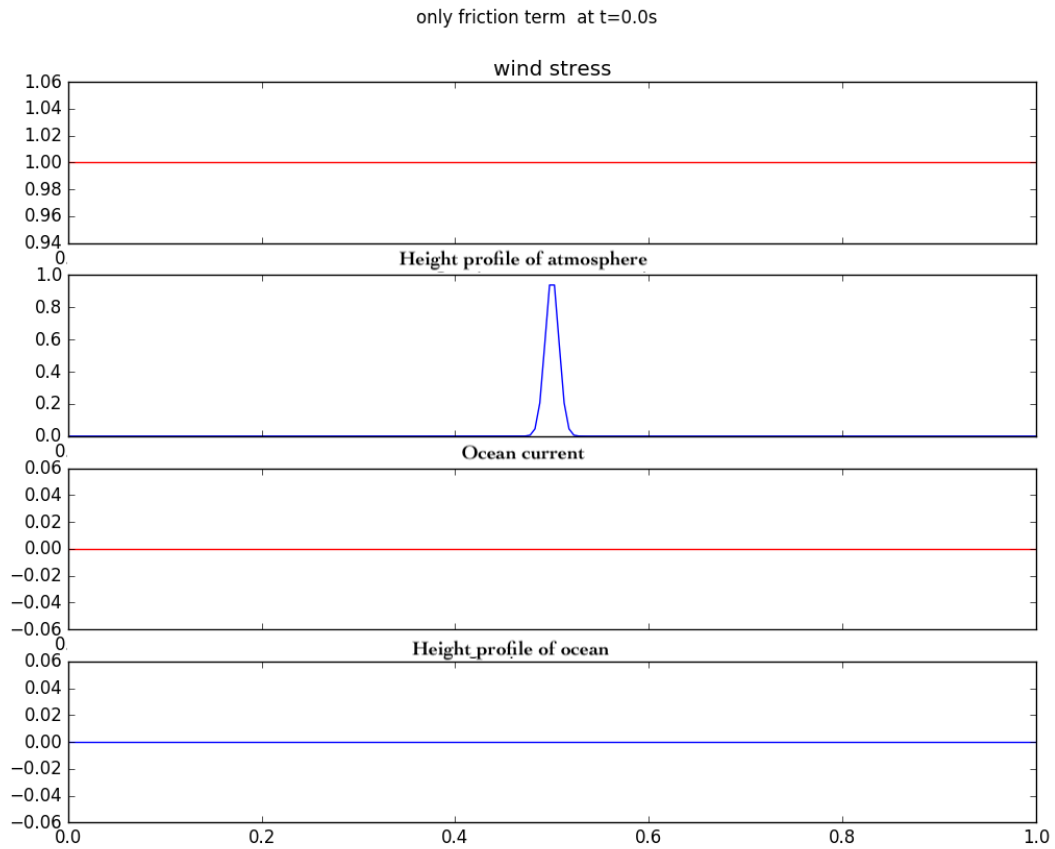
Figure A.5: Initial conditions of velocity and height for atmosphere and ocean. x axis denotes the domain and y axis denotes the velocity and height profile of atmosphere and ocean.
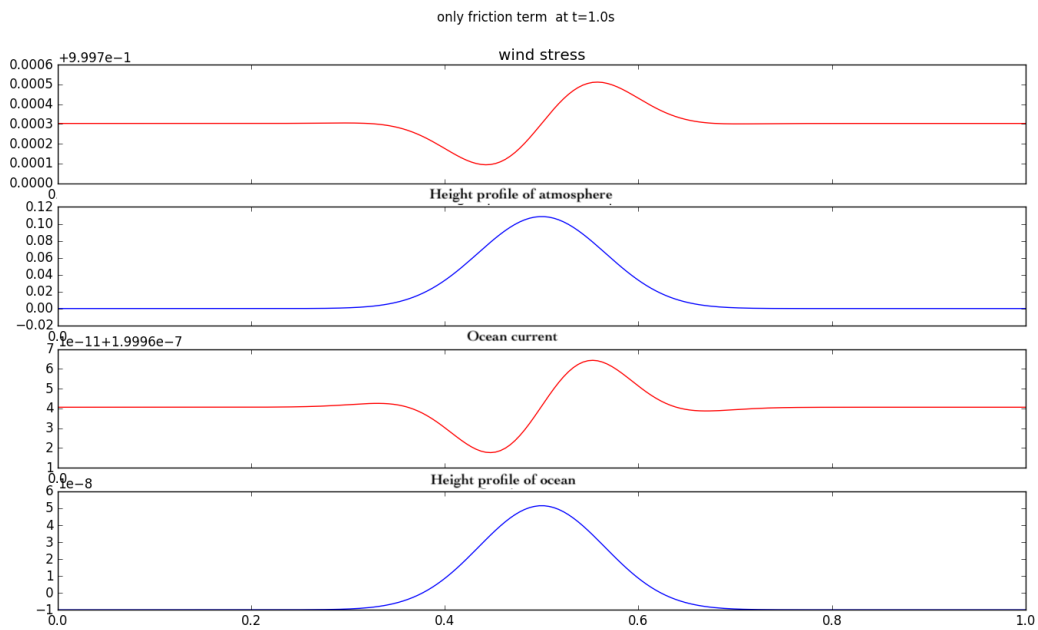
Figure A.6: One way interaction between atmosphere and ocean through momentum flux. x axis denotes the domain and y axis denotes the velocity and height profile of atmosphere and ocean.
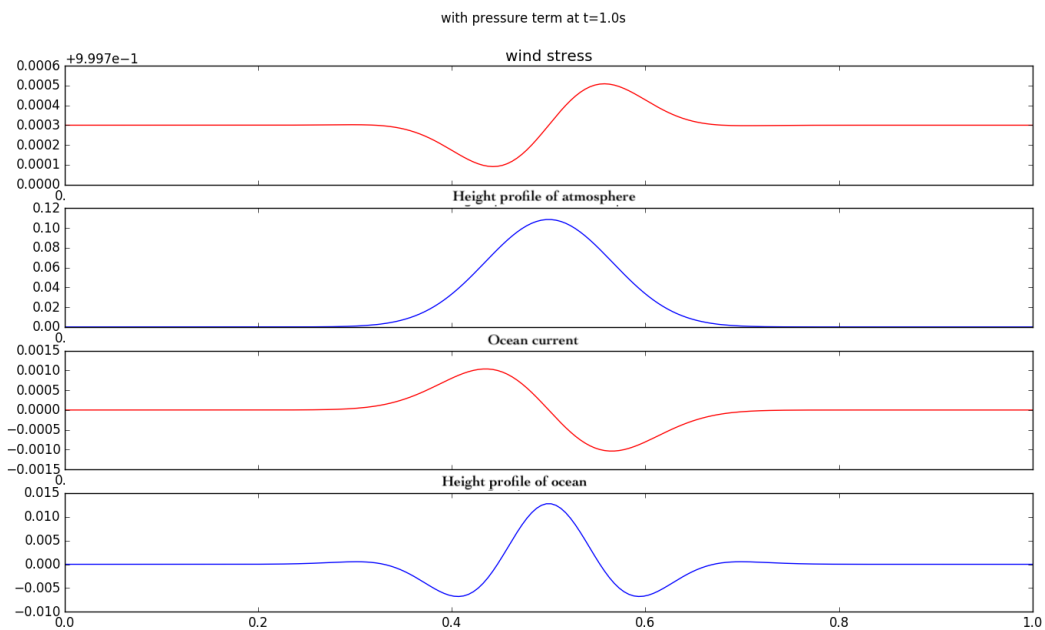

Figure A.7: Effect of pressure forcing term on ocean. x axis denotes the domain and y axis denotes the velocity and height profile of atmosphere and ocean.

Appendix B

Coupling Strategies we tried

B.1   Introduction

After we tested our coupling ideas to equations with a fixed interface in Appendix A as a preliminary result, we further tested our coupling idea to couple 1D diffusion equation with different diffusion coefficients with a moving boundary at the interface. From the literature, we found a interface condition (B.1) from [58] which couples diffusion equations with different diffusion coefficients at the interface, thereby computes interface temperature. However, this equation computes interface temperature for a fixed interface. This Chapter describes our failed idea to implement moving boundary at the interface. As a preliminary result, we considered coupling equation for the fixed interface to couple diffusion equations. Then in order to move the interface, we used a criteria at the interface: When the interface temperature is greater than melting temperature, we consider that the interface position moves to the right side of the domain resulting in melting of the solid domain. When the interface temperature is less than the melting temperature, we considered that interface position moves to the left representing freezing of liquid domain. We implemented these ideas to two coupling methods., say loose and tight coupling. In loose coupling, we consider one grid point overlap between the subdomains. In addition, we implemented tight coupling where we considered larger overlap with five grid point overlap. We realise that the coupling equation (B.1) for a moving interface and our criteria to move the interface is not accurate, however we think that it is important to document our failed ideas. Since our results in

this Chapter are only the implementation of our failed ideas, we do not proceed further to analyse these results with the Stefan problem (reference).

The heat equation for liquid and solid domains is same as in (2.35) and (2.36) respectively. As a preliminary result, we used the coupling equation (B.1) for the fixed interface from the literature [58]

$$\frac{\partial u}{\partial t} = (k_s \frac{\partial u}{\partial x} - k_l \frac{\partial u}{\partial x}). \tag{B.1}$$

However, the equation (B.1) is not suitable for our case, as we are dealing with a moving interface. As a result, we derived the coupling using First principle approach, described in chapter 3 and 4. In the further sections, we explained loose and tight coupling methods we tried using the above equation (B.1).

B.2   Coupling methods tried

B.2.1   Loose Coupling

We discretize the diffusion equation using forward in time and centred difference in space similar to 2.65 and 2.66. Let ib is the index at the interface. At the interface, we discretise the equation B.1, however the equation B.1 does not fit to our moving interface and thereby we use the equation 3.15 in chapter 3

The numerical algorithm for diffusion equation (2.35) in liquid domain:

$$\frac{(u_i^{n+1} - u_i^n)}{\Delta t} = \frac{k_l}{(\Delta x)^2}(u_{i+1}^n - 2u_i^n + u_{i-1}^n) \tag{B.2}$$

The numerical algorithm for diffusion equation (2.36) in solid domain is:

$$\frac{(u_i^{n+1} - u_i^n)}{\Delta t} = \frac{k_s}{(\Delta x)^2}(u_{i+1}^n - 2u_i^n + u_{i-1}^n) \tag{B.3}$$

The numerical algorithm at the interface to compute the temperature at the interface,

$$\frac{(u_{ib}^{n+1} - u_{ib}^n)}{\Delta t} = \frac{k_s}{\Delta x}(u_{ib+1}^n - u_{ib}^n) - \frac{k_l}{\Delta x}(u_{ib}^n - u_{ib-1}^n) \tag{B.4}$$

where Δt and Δx are the temporal and spatial step size respectively. The interface temperature (u_{ib}^{n+1}) obtained from (B.4) is for fixed interface. In order to move the interface, we used the following condition:

```
if  uib^n+1  ≥  um  :
     ib  =  ib+1
elif  uib^n+1  <  um  :
     ib  =  ib-1
```

If the interface temperature is greater than melting temperature, we consider it to move to right of the domain resulting in melting. If not, to the left showing freezing. However this process of moving the interface position may not be correct and the correction of this method is described in chapter 3.

B.2.2   Implicit Algorithm for coupling

We consider an algorithm which i implicit on both sides of the interface, but with explicit updating of the data used at the interface. The numerical algorithm for diffusion equation (2.35) in liquid domain:

$$\frac{(u_i^{n+1} - u_i^n)}{\Delta t} = \frac{k_l}{(\Delta x)^2}(u_{i+1}^n - 2u_i^n + u_{i-1}^n) \tag{B.5}$$

The numerical algorithm for diffusion equation (2.36) in solid domain is:

$$\frac{(u_i^{n+1} - u_i^n)}{\Delta t} = \frac{k_s}{(\Delta x)^2}(u_{i+1}^n - 2u_i^n + u_{i-1}^n) \tag{B.6}$$

The numerical algorithm at the interface to compute the temperature at the interface,

$$\frac{(u_{ib}^{n+1} - u_{ib}^n)}{\Delta t} = \frac{k_s}{\Delta x}(u_{ib+1}^n - u_{ib}^n) - \frac{k_l}{\Delta x}(u_{ib}^{n+1} - u_{ib-1}^{n+1}) \tag{B.7}$$

The interface temperature (u_{ib}^{n+1}) obtained from (B.7) is for fixed interface. In order to move the interface, we used the following condition:
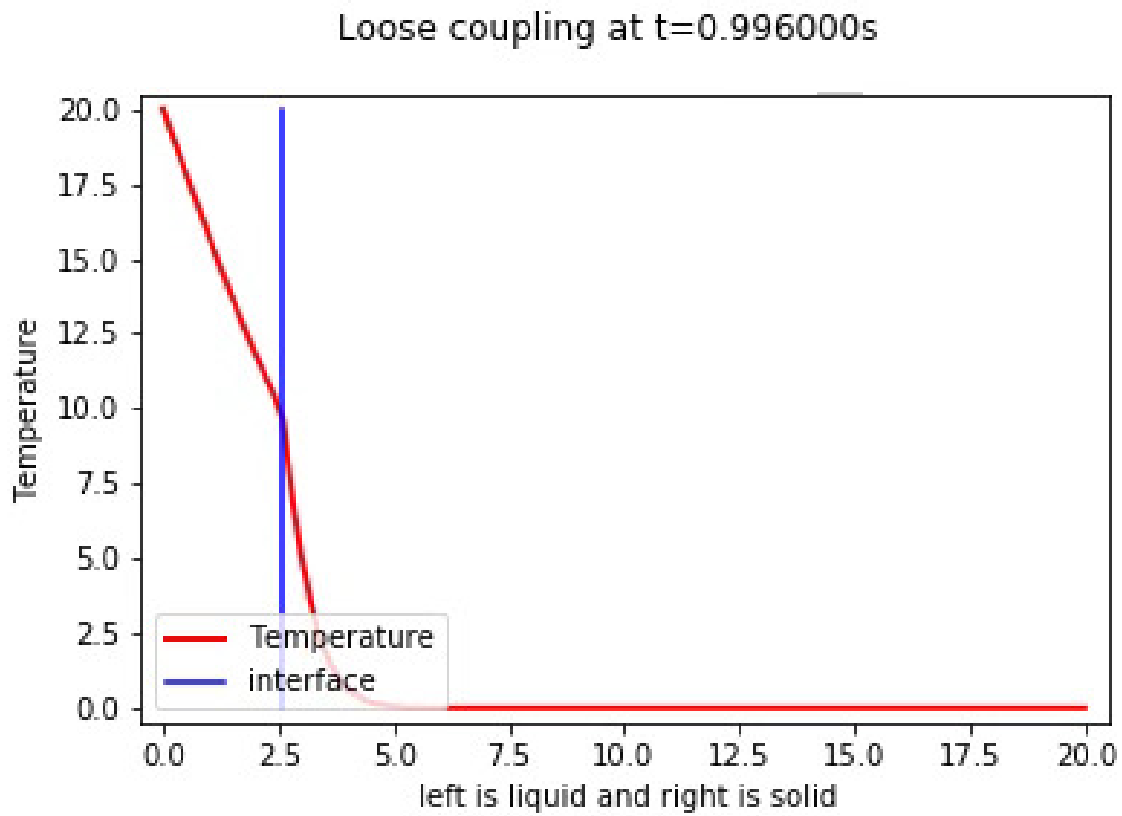
Figure B.1: Solution of loose coupling method using explicit method at t ≈ 1. Red line represents diffusion of temperature and blue line represents the position of interface

```
if  u_{ib}^{n+1}  ≥  u_m  :
    ib  =  ib+1
elif  u_{ib}^{n+1}  <  u_m  :
    ib  =  ib-1
```

However this process of moving the interface position to one grid point may not be correct and the correction of this method is described in chapter 3.

B.3   Tight Coupling

In order to achieve higher order accuracy, better approximations of the derivatives are used. We consider fourth order central difference approximations for first order derivatives to calculate solid and liquid fluxes. These approximations use five point stencils in 1D. We consider forward in time and centred difference in space for discretization of solid and liquid domains.

The numerical algorithm for diffusion equation (2.35) in liquid domain:

$$\frac{(u_i^{n+1} - u_i^n)}{\Delta t} = \frac{k_l}{(\Delta x)^2}(u_{i+1}^n - 2u_i^n + u_{i-1}^n) \tag{B.8}$$

The numerical algorithm for diffusion equation (2.36) in solid domain is:

$$\frac{(u_i^{n+1} - u_i^n)}{\Delta t} = \frac{k_s}{(\Delta x)^2}(u_{i+1}^n - 2u_i^n + u_{i-1}^n) \tag{B.9}$$

At the interface, we consider the higher order derivative over the interface, but this is not really defined, since there is a phase change at the interface, which is mathematically a discontinuity (at least in the derivative). So, what we did was that we compared the left side derivative with the right side derivative.

$$\frac{\Delta x}{\Delta t}(u_{ib}^{n+1} - u_{ib}^n) = \frac{k_s}{\Delta x}\left(\frac{u_{ib-2}^n}{12} - 2\frac{u_{ib-1}^n}{3} - 2\frac{u_{ib+1}^n}{3} + \frac{u_{ib+2}^n}{12}\right) - \frac{k_l}{\Delta x}\left(\frac{u_{ib-2}^n}{12} - 2\frac{u_{ib-1}^n}{3} - 2\frac{u_{ib+1}^n}{3} + \frac{u_{ib+2}^n}{12}\right), i = ib \tag{B.10}$$

In order to change the position of the interface based on the interface temperature, we used the following code at the interface.
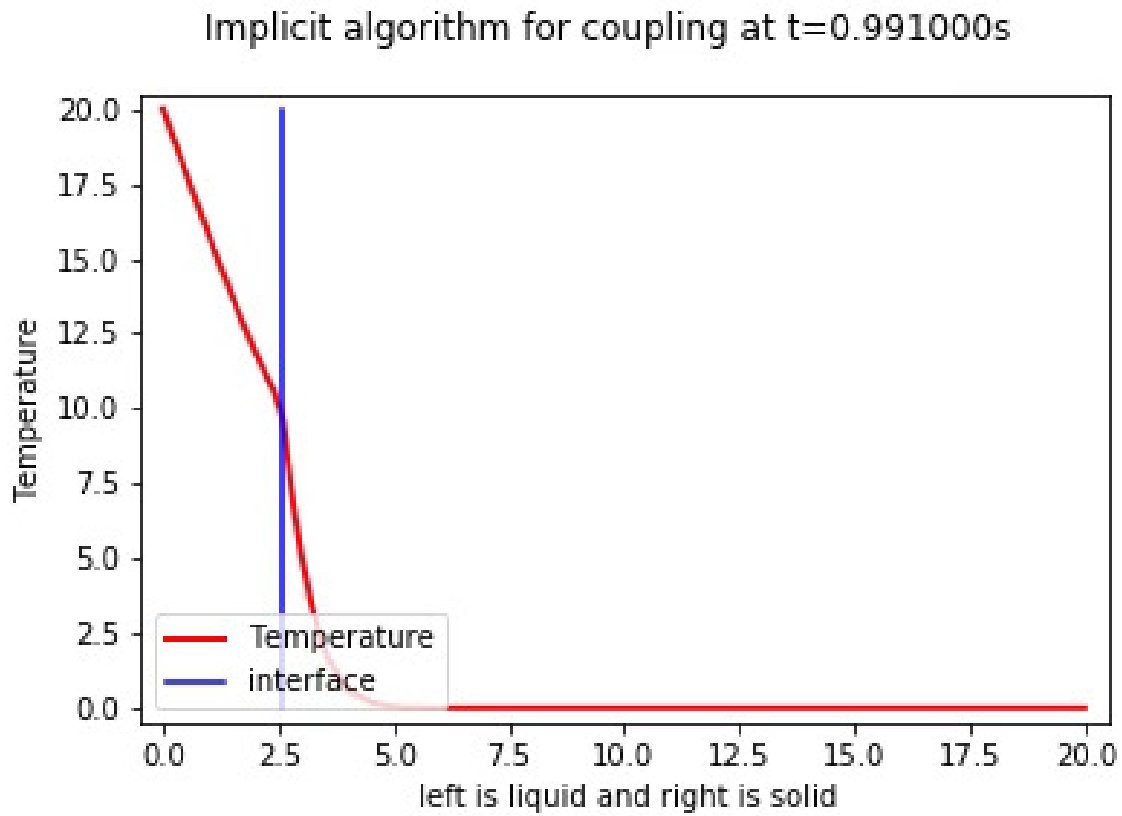
Figure B.2: Solution of loose coupling method using implicit method at t ≈ 1. Red line represents diffusion of temperature and blue line represents the position of interface

```
if  u_ib^{n+1} ≥ u_m  :
    ib  =  ib+1
elif  u_ib^{n+1} < u_m  :
    ib  =  ib-1
```

B.4   Problems Encountered

We have encountered some problems in the implementation of the interface condition (B.1) in these coupling methods. The Stefan condition (2.38) is used to determine the new interface position s(t) based on the temperature gradients of liquid and solid domains. Whereas the interface condition (B.1) in the coupling methods computes the temperature at the fixed interface based on exchanging fluxes at the interface [58]. In order to compare the results of coupling methods to solution of Stefan problem, the interface position in (B.1) should move. In order to move the position of interface, we used a criteria in this Chapter. However, it is not accurate and therefore we derived a coupling equation (3.15) based on first principle approach, where interface temperature is computed for a moving interface. We then compared the results of our coupling methods to the solution of Stefan problem further explained in Chapter 4.

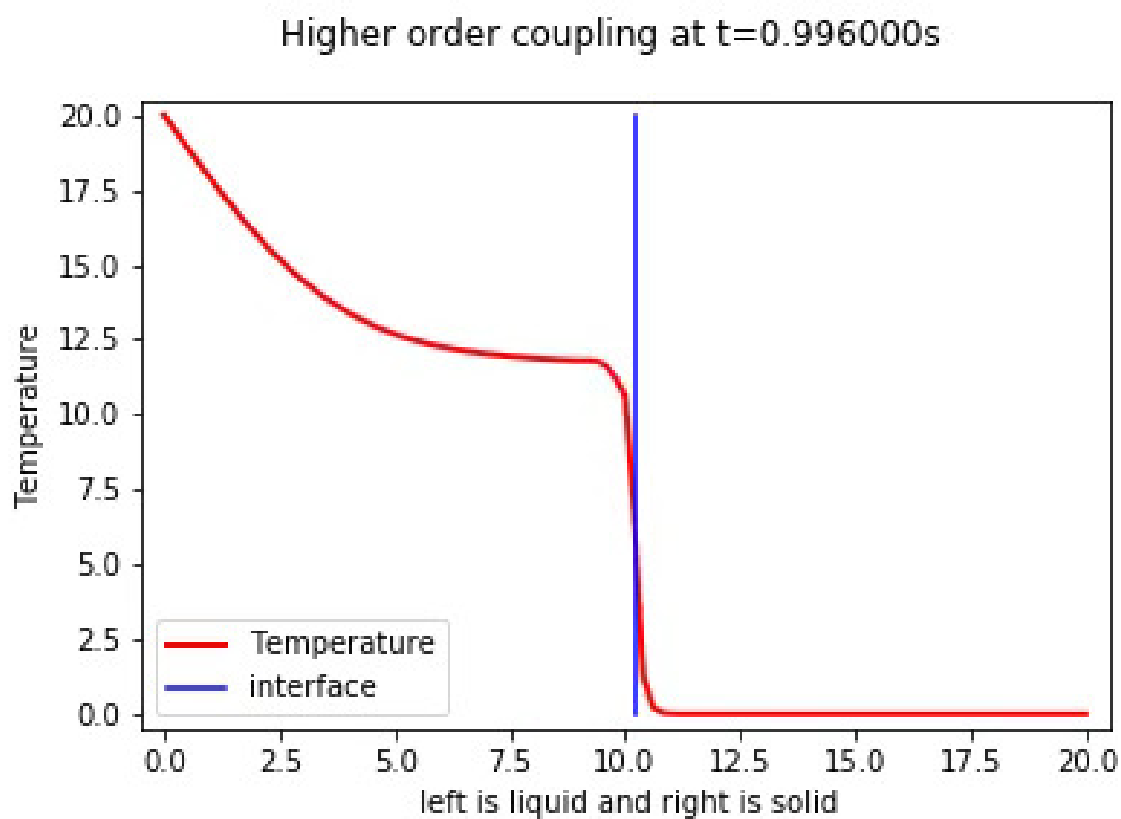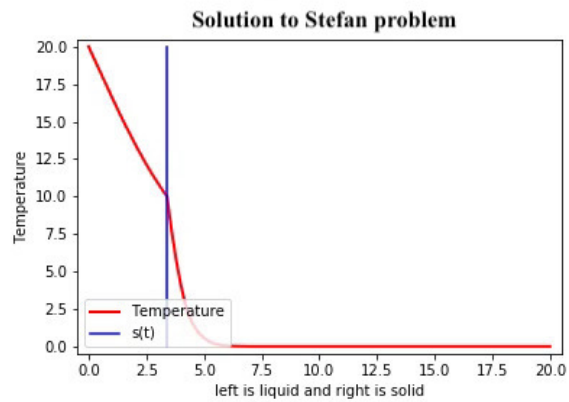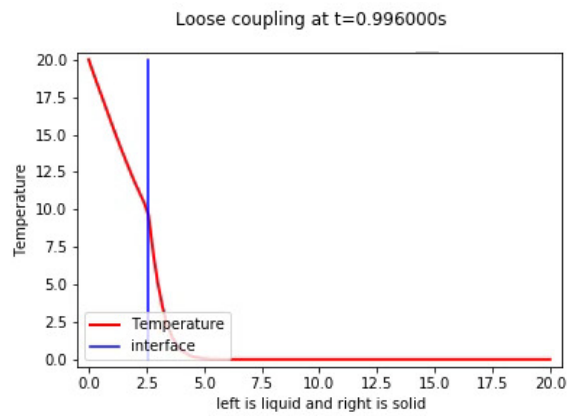Figure B.3: Solution of tight coupling method at t ≈ 1. Red line represents diffusion of temperature and blue line represents the position of interface
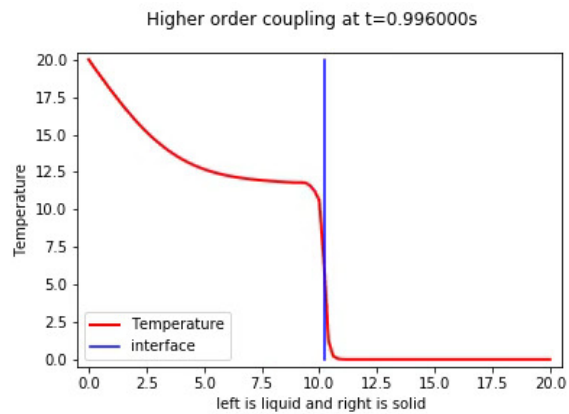
Figure B.4: Comparing the results of (a) Numerical solution of two phase Stefan problem, (b) solution of loose coupling, (c) solution of tight coupling at $t \approx 1$. The red line represents temperature and the blue line represents the position of the interface.

Bibliography

[1] Roeckner, E., Bäuml, G., Bonaventura, L., Brokopf, R., Esch, M., Giorgetta, M., Hagemann, S., Kirchner, I., Kornblueh, L., Manzini, E., Rhodin, A., Schlese, U., Schulzweida, U and Tompkins, A., *The atmospheric general circulation model ECHAM 5. PART I: Model description*, Rep. 349, MPI für Meteorol, Hamburg, Germany., (2003)

[2] Jungclaus, J. H., Fischer, N., Haak, H., Lohmann, K., Marotzke, J., Matei, D., Mikolajewicz, U., Notz, D and von Storch, J. S; *Characteristics of the ocean simulations in the Max Planck Institute Ocean Model (MPIOM), the ocean component of the MPI- Earth system model*, J. Adv. Model. Earth Syst., **5**: 422–446 (2013)

[3] Maier-Reimer, E., *Geochemical cycles in an ocean general circulation model: Preindurstrial tracer distributions*, Global Biogeochem. Cycles., **7**: 645–677 (1993)

[4] Hibler, W. D., *A dynamic thermodynamic sea ice model*, J. Phys. Oceanogr., **9**: 815–846 (1979)

[5] Marsland, S. J., Haak, H., Jungclaus, J. H., Latif, M and Röske, F; *The Max-Planck-Institute global ocean/sea ice model with orthogonal curvilinear coordinates*, Ocean Modell., **5**: 91–127 (2003)

[6] Avissar, R and Pielke, R. A., *A parameterization of heterogeneous land surfaces for atmospheric numerical models and its impact on regional meteorology*, Mon. Weather Rev., **117**: 2113–2136 (1989)

[7] Valcke, S., Balaji, V., Craig, A., Deluca, C., Dunlap, R., Ford, R. W., Jacob, R., Larson, J., O'Kuinghttons, R., Riley, G. D and Vertenstein, M., *Coupling technologies for Earth System Modelling*, Geosci. Model Dev., **5**: 1589–1596 (2012)

[8] Craig, A., Valcke, S and Coquart, L., *Development and performance of a new version of the OASIS coupler, OASIS3-MCT3.0*, Geosci. Model Dev., **10**: 3297–3308 (2017)

[9] Lemarié, F., Blayo E and Debreu L., *Analysis of ocean-atmosphere coupling algorithms: consistency and stability*, Procedia Comput. Sci., **51**: 2066–2075 (2015)

[10] Lemarié, F., Debreu, L and Blayo, E., *Toward an optimized global-in-time Schwarz algorithm for diffusion equations with discontinuous and spatially variable coefficients part 1 : the constant coefficients case*, Electron. Trans. Numer. Anal., **40**: 148–169 (2013)

[11] Lemarié, F., Debreu, L and Blayo, E., *Toward an optimized global-in-time Schwarz algorithmfor diffusion equations with discontinuous and spatially variable coefficients, part 2 : the variable coefficients case*, Electron. Trans. Numer. Anal., **40**: 170–186 (2013)

[12] Gander, M. J., Halpern, L and Kern, M., *A Schwarz waveform relaxation method for advection-diffusion-reaction problems with discontinuous coefficients and non-matching grids*, Domain decomposition methods in science and engineering XVI, **55**: 283–290 (2007)

[13] Gander, M. J., *Schwarz methods over the course of time*, Electron. Trans. Numer. Anal., **31**: 228–255 (2008)

[14] Canuto, C and Funaro, D., *The Schwarz algorithm for spectral methods*, SIAM J. Numer. Anal., **25**: 24–40 (1988)

[15] Ledley, T. S., *Snow on sea ice: Competing effects in shaping climate*, J. Geophys. Res., **96**: 17,195–17,208 (1991)

[16] Brandt, R. E., Warren, S. G., Worby, A. P and Grenfell, T. C., *Surface albedo of the Antarctic sea ice zone*, J. Climate., **18**: 3606–3622 (2005)

[17] Zwally, H. J., Abdalati, W., Herring, T., Larson, K., Saba, J and Steffen, K., *Surface melt induced acceleration of Greenland ice-sheet flow*, Science., **297**: 218–222 (2002)

[18] Lenaerts, J. T. M., van den Broeke, M. R., van Angelen, J. H., van Meijgaard, E and Déry, S. J., *Drifting snow climate of the Greenland Ice Sheet: A study with a regional climate model*, The Cryosphere., **6**: 891–899 (2012)

[19] Benn, D. I and Evans, D. J. A., *Glaciers and glaciation*, 2nd edition (2nd ed.), Routledge., (2010)

[20] Hubbard, B., *Direct measurement of basal motion at a hard-bedded, temperate glacier: Glacier de Tsanfleuron, Switzerland*, J. Glaciol., **48**: 1–8 (2002)

[21] Watson, C. S. and Quincey, D., *Glacier Movement*, Geomorphological Techniques, Chapter. 3, British Society for Geomorphology (L. E. Clarke, J. M. Nield, eds)., pp. 13 (1987)

[22] Stefan, J., *Über die Theorie der Eisbildung, inbesondere über die Eisbildung im Polarmeer*, Ann. Phys. Chem., **278**: 269–286 (1891)

[23] Andreucci, D., *Lecture notes on the Stefan problem.*, "http://www.sbai.uniroma1.it/pubblicazioni/doc/phd_quaderni/02-1-and.pdf", (2002)., [Online; accessed 05-April-2022]

[24] Alexiades, V and Solomon, A. D., *Mathematical modelling of melting and freezing Processes*, Hemisphere Publication, Washington DC., (1993)

[25] Boucíguez, A. C., Lozano, R. F and Lara, M. A., *About the exact solution in two phase Stefan problem*, Engenharia Térmica., **6**: 70–75 (2007)

[26] Sein, D. V., Mikolajewicz, U., Gröger, M., Fast. I and Cabos, W., Pinto, J, G., Hagemann, S., Semmler, T., Izquierdo, A and Jacob, D., *Regionally coupled atmosphere-ocean-sea ice-marine biogeochemistry model ROM. Part I: Description and validation*, J. Adv. Model. Earth Syst., **7**: 268–304 (2015)

[27] Balaji, V., Held, I., Winton, M., Durachta, J., Malyshev. S and Stouffer, R., *The Exchange Grid: A mechanism for data exchange between Earth System components on independent grids*, Parallel computational fluid dynamics, Elsevier., pp. 179–186 (2006)

[28] Roeckner, E., Arpe, K., Bengtsson, L., Christoph, M., Claussen, M., Dümenil, L., Esch, M., Giorgetta, M., Schlese, U and Schulzweida U., *The atmospheric general circulation model ECHAM-4: Model description and simulation of present-day climate*, Rep. 218, MPI für Meteorol, Hamburg, Germany., (1996)

[29] Maier-Reimer, E., Kriest, I., Segschneider, J and Wetzel P., *The Hamburg ocean carbon cycle model, HAMOCC5.1. Technical description*, Reports on Earth System Science, Max Planck Institute for Meteorol., Hamburg., (2005)

[30] Fairall, C. W., Bradley, E. F., Rogers, D. P., Edson, J. B and Young, G. S., *Bulk parameterization of air-sea fluxes for Tropical Ocean-Global Atmosphere Coupled-Ocean Atmosphere Response Experiment*, J. Geophys. Res., **101**: 3747–3764 (1996)

[31] Legutke, S and Voss, R., *The Hamburg Atmosphere-Ocean Coupled Circulation Model ECHO-G*, Tech. Rep. 18, World Data Center for Climate (WDCC), DKRZ., (1999)

[32] Blayo, E., Halpern, L and Japhet, C., *Optimized Schwarz waveform relaxation algorithms with nonconforming time discretization for coupling convection-diffusion problems with discontinuous coefficients*, Domain Decomposition Methods in Science and Engineering XVI (Olof B. W and Walter Z, eds), 55, Springer Verlag., pp. 267-274 (2007)

[33] Cai X., *Overlapping Domain Decomposition Methods*, Advanced Topics in Computational Partial Differential Equations, Lecture Notes in Computational Science and Engineering (Langtangen H.P., Tveito A. eds), 33, Springer, Berlin, Heidelberg., (2003)

[34] Sen, N., Sungho S., Mihai A and Victor M. Z., *On the Convergence of Overlapping Schwarz Decomposition for Nonlinear Optimal Control*, arXiv:2005.06674v5., (2020)

[35] Tony, F. C and Tarek, P. M., *Domain decomposition algorithms*, Acta Numerica., pp. 61–143 (1994)

[36] Lions, P. L., *On the Schwarz alternating method I*, First international symposium on Domain Decomposition methods for partial differential equations, SIAM, Philadelphia, pp. 1-42., (1988)

[37] Lions, P. L., *On the Schwarz alternating method. III: a variant for nonoverlapping subdomains*, Third international symposium on Domain Decomposition methods for partial differential equations, SIAM, Philadelphai, pp. 202-223., (1990)

[38] Gurevich, S., *Numerical methods lectures Chapter 7 - The Diffusion Equation.*, "https://www.uni-muenster.de/imperia/md/content/physik_tp/lectures/ws2016-2017/num_methods_i/heat.pdf", (Winter semester 2016-2017)., [Online; accessed 14-September-2021]

[39] Matthew, J. H., *The 1D Heat Equation 18.303 Linear Partial Differential Equations*, "https://ocw.mit.edu/courses/mathematics/18-303-linear-partial-differential-equations-fall-2006/lecture-notes/heateqni.pdf", (Fall 2006)., [Online; accessed 14-September-2021]

[40] Rubinstein, L.I., *The Stefan Problem*, J. Am. Math. Soc, Providence, Rhode Island., (1971)

[41] Jonsson, T., *On the one dimensional Stefan problem with some numerical analysis*, "https://www.diva-portal.org/smash/get/diva2:647481/FULLTEXT01.pdf, Umeå Universität, (Spring 2013)., [Online., accessed 07-April 2022]

[42] Morgan, F., *Real Analysis and Applications*, American Mathematical Society, Providence, Rhode Island., (2005)

[43] Notz, D and Bitz, C. M., *Sea ice in Earth system models*, Sea Ice, 3rd edition (3rd ed.), pp. 304-329 (2016)

[44] Hunk, E. C., Lipscomb, W. H and Turner, A. K., *Sea-ice models for climate study: retrospective and new directions*, J. Glaciol., **56**: 1162–1172 (2010)

[45] Semmler, T., Jacob, D., Schlünzen, K. H and Podzun R., *Influence of sea ice treatment in a regional climate model on boundary layer values in the Fram Strait region*, Mon. Weather Rev., **132**: 985–999 (2004)

[46] Stössel, A and Owens, W. B., *The Hamburg sea-ice model*, Tech. Rep. 3, World Data Center for Climate (WDCC), DKRZ., (1992)

[47] Notz, D., *Challenges in Simulating Sea Ice in Earth System Models*, Wiley Interdiscip. Rev. Clim. Change., **3**: 509–526 (2012)

[48] Omstedt, A., *A coupled one-dimensional sea-ice-ocean model applied to a semi enclosed basin*, Tellus A: Dyn. Meteorol. Oceanogr., **42**: 568–582 (1989)

[49] Ohshima, K. I., Yoshida, K., Shimoda, H., Wakatsuchi, M., Endoh, T and Fukuchi, M., *Relationship between the upper ocean and sea ice during the Antarctic melting season*, J. Geophys. Res., **103**: 7601–7615 (1998)

[50] Komuro, Y and Hasumi, H., *Effects of surface freshwater flux induced by sea ice transport on the global thermohaline circulation*, J. Geophys. Res., **108**: 3047 (2003)

[51] Bitz, C. M and Lipscomb, W. H., *An energy-conserving thermodynamic model of sea ice*, J. Geophys. Res., **104**: 15,669–15,677 (1999)

[52] Ebert, E. E and Curry, J. A., *An intermediate one-dimensional thermodynamic sea-ice model for investigating ice-atmosphere interaction*, J. Geophys. Res., **98**: 10085–10109 (1993)

[53] Gabison, R., *A thermodynamic model of the formation, growth and decay of first year sea-ice*, J. Glaciol., **33**: 105–119 (1987)

[54] Maykut, G.A and Untersteiner, N., *Some results from a time dependent thermodynamic model of sea-ice*, J. Geophys. Res., **76**: 1550–1575 (1971)

[55] Semtner, A. J., *A model for the thermodynamic growth of sea-ice in numerical investigation of climate*, J. Phys. Oceanogr., **6**: 379–389 (1976)

[56] Flato, G. M and Brown, R. D, *Variability and climate sensitivity of landfast Arctic sea ice*, J. Geophys. Res., **101**: 25767–25777 (1996)

[57] Launiainen, J and Cheng B., *Modelling of ice thermodynamics in natural water bodies*, Cold. Reg. Sci. Technol., **27**: 153–178 (1998)

[58] Giles, M. B., *Stability analysis of numerical interface conditions in fluid structure thermal analysis*, Int. J. Num. Meth. Fluids., **25**: 421–436 (1997)

[59] Staniforth, A., Wood, N and Côté, J., *Analysis of the numerics of physics-dynamics coupling*, Q. J. R. Meteorol. Soc., **128**: 2779–2799 (2002)

[60] Staniforth, A., Wood, N and Côté, J., *A simple comparison of four physics dynamics coupling schemes*, Mon. Weather Rev., **130**: 3129–3135 (2002)

[61] Canuto, C., Hussaini, M., Quarteroni, A and Zang, T., *Spectral methods in Fluid Dynamics*, Springer, Berlin., (1988)

[62] Lions, P. L., *On the Schwarz alternating method II*, Stochastic Interpretation and Order Proprieties (T. F. Chan, et al., eds), Domain Decomposition Methods, SIAM, Philadelphia, pp. 47-70., (1989)

[63] Smith, B., Bjørstad, P and Gropp, W., *Domain Decomposition: Parallel multilevel methods for elliptic partial differential equations*, Cambridge University Press, Cambridge., (1996)

[64] Levy.D., *Interpolation*, "https://wiki.math.ntnu.no/_media/ma8502/2014h/interpolation-levy.pdf"., [Online; accessed 15-February-2022]

[65] Wikipedia contributors., *Linear interpolation–Wikipedia, The Free Encyclopedia*, "https://en.wikipedia.org/w/index.php?title=Linear_interpolation&oldid=1064278127", (enwiki:1064278127)., [Online; accessed 15-February-2022]

[66] Anderson, C. R., *Domain Decomposition techniques and the solution of Poisson's equation in infinite Domains*, in Domain Decomposition Methods (T. Chan, R. Glowinski, J. Periaux, and O. Widlund, eds), SIAM, Philadelphia., (1989)

[67] Meurant, G. A., *A domain decomposition method for parabolic problems*, Applied Numeric Math., **8**: 427–441 (1991)

[68] Moulin, A and Wirth, A., *A drag-induced barotropic instability in air-sea interaction*, J. Phys. Oceanogr., **44**: 733–741 (2014)

[69] Moulin, A and Wirth, A., *Momentum transfer between an atmospheric and an oceanic layer at the synoptic and the mesoscale: An idealized numerical study*, Boundary-Layer Meteorol., **160**: 551–568 (2016)

[70] Zanolli, P., *Domain Decomposition algorithms for spectral methods*, Calcolo., **24**: 201–240 (1987)

[71] Schwarz, H. A., *Über einen GrenzÜbergang durch alternierendes Verfahren*, Vierteljahrsschrift der Naturforschenden Gesellschaft in Zürich., **15**: 272–286 (1870)

[72] Stull, R. B., *An introduction to boundary layer meteorology*, Ekluwer Academic Publishers, Dordrecht., pp. 666 (1988)

[73] Proudman, J., *The effects on the sea of changes in atmospheric pressure*, Geophys. Suppl. Mon. Notices Royal Astron. Soc., **2**: 197–209 (1929)